Available online at www.sciencedirect.com

ScienceDirect

Advances in Space Research 66 (2020) 2487–2515

ADVANCES IN SPACE RESEARCH (a COSPAR publication)

www.elsevier.com/locate/asr

Review

Long polar motion series: Facts and insights

Gerhard Beutler, Arturo Villiger *, Rolf Dach, Andreas Verdun, Adrian Jäggi

Astronomical Institute of the University of Bern, Sidlerstrasse 5, 3012 Bern, Switzerland

Received 9 April 2020; received in revised form 25 August 2020; accepted 27 August 2020
Available online 17 September 2020

Abstract

Polar motion (PM) series from various observation methods and sources are analyzed using one and the same simple analysis tool. The maximum time resolution of the Earth Rotation Parameter (ERP) series considered here is one day, which leaves out ERP series with sub-daily time resolution. A longer spacing between subsequent epochs is permissible, a variable spacing between epochs like in the VLBI (Very Long Baseline Interferometry) series as well. The shortest length of the PM time series analyzed, based on GNSS (Global Navigation Satellite Systems), is 26+ years, the longest one, the IERS C01 series, 173+ years.

Following the tradition, PM is decomposed into a mean motion, i.e., the motion of the center of the PM curve on the surface of the Earth, a prograde Chandler motion with a nominal period of 432.25 days, and a prograde annual motion with a nominal period of 365.25 days. In our analysis, Secular PM is not assumed as linear, but as piecewise linear and continuous. The defining parameters of the periodic parts of polar motion are not assumed as constant either, but as piecewise linear and continuous functions of time as well. All parameters of the PM model based on one particular ERP series are determined in one and the same linear least squares estimation. Parameters of the same type may be purely deterministic or filtered (smoothed) by constraining the second time differences of the parameters (the second time derivative of the parameter functions) of the same kind.

The key results achieved by applying our method to a wide variety of ERP series are visualized and discussed. They include: (a) the description of a sharp bend of mean PM around 1996, (b) strong evidence for a multi-component model for Chandler motion with periods separated by few days, similar to that proposed by Chandler (1901), (c) a reconstruction of mean PM from 1846 to present taking into account the composite nature of the series, and (d) a prediction of Chandler motion for the next decades.

A sharp bend of mean PM was found around 1995/96, along the meridian at about 70° West to the meridian at about 12–15° West. All PM curves analyzed show a mean motion in this new direction after 1995/95. Smaller excursions w.r.t.d this mean exist, with periods < 10 years. A periodic variation with a period of about 180 years was observed in the Chandler signal of PM with an amplitude of more than 200 mas. The variation may be explained approximately by a composite nature of Chandler motion, similar to the model already proposed by Chandler (1901). This simple model was generalized using a Fourier series separated in period by few days. This alternative model of Chandler motion is used to predict the Chandler part of PM, with an amplitude close to zero currently, to reach values of the order of 100 mas around 2028–2030.

Keywords: Polar motion (PM); GNSS; DORIS; SLR; VLBI; Astrometry

* Corresponding author.
E-mail address: arturo.villiger@aiub.unibe.ch (A. Villiger).

https://doi.org/10.1016/j.asr.2020.08.033
0273-1177/

Contents

1. Introduction: illustration, principles, and overview

Loosely speaking, Polar Motion (PM) marks the motion of the Earth's rotation axis on the Earth's surface. According to the IERS Conventions 2010 (Petit and Luzum, 2010) "polar motion is the motion of the Earth's pole w.r.t. the ITRS[1]", more precisely, of the Earth's rotation pole w.r.t. the ITRS North pole.

The PM components x and y are defined as the angular distances of the Earth's rotation axis from the ITRS North pole, measured along two mutually orthogonal meridians. They are the angles in the rotation matrices $R_1(y)R_2(x)$ in the transformation from the terrestrial to the inertial system. The right-handed coordinate system $(l = x, m = -y)$ initiated by Jeffreys (1940) will be used, subsequently. Its l-axis lies on the Greenwich meridian, its m-axis on the meridian at Eastern longitude $\lambda = 90°$. When representing the polar coordinates as a function of time, the traditional coordinates x and y will be used.

Illustration. Fig. 1 (top) illustrates PM from the CODE solution (Dach et al., 2009) between 2000.0 and 2006.5 as the black curve in this coordinate system in units of milliarcseconds (mas). The start- and end-epochs are marked with a green and magenta dot, respectively. The figure also shows the motion of the mean pole[2] derived from the CODE series between 1993.6 and 2020.0 as the red curve. The comparison of the black and the red curves in Fig. 1

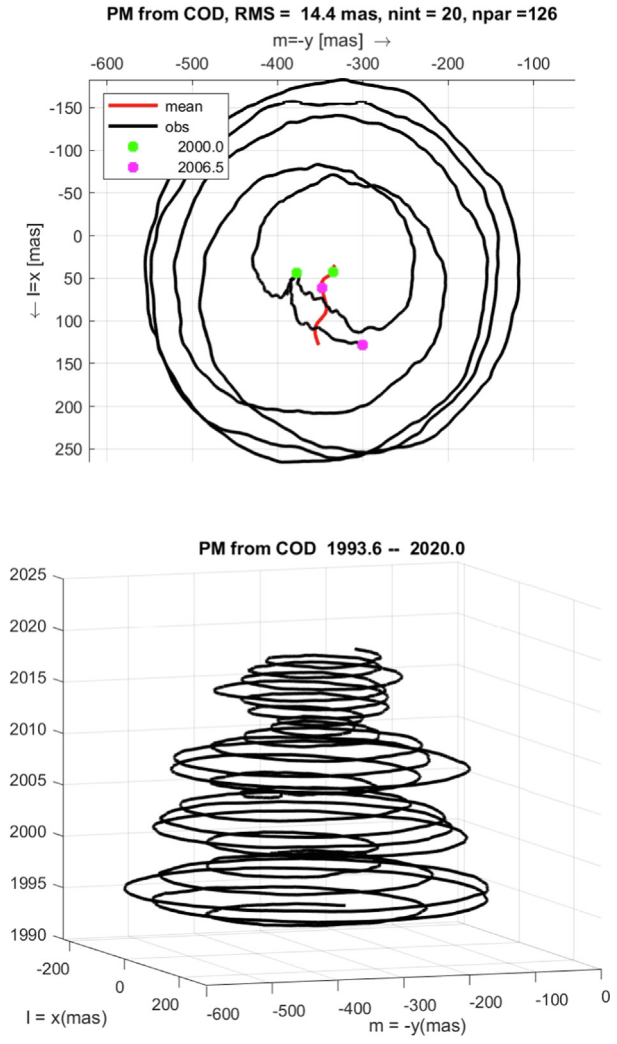

Fig. 1. Top: CODE PM in mas between 2000.0 and 2006.4, bottom: CODE PM in mas from 1993.6 to 2020.0 as a 3-dimensional illustration; time in years on the third coordinate axis.

[1] International Terrestrial Reference System

[2] The term *mean pole* is used throughout this article as defined in the update (http://iers-conventions.obspm.fr/content/iccgl.pdf) to the IERS Conventiones 2010 (Petit and Luzum, 2010). In abbreviated form this definition says: "the mean pole represents the low-frequency motion of the Earth's rotation axis with respect to the terrestrial reference system; it is free of the principal periodic motions (Chandler and annual)."

(top) indicates that the extraction of the mean pole from the observed PM values is far from trivial.

Fig. 1 (bottom) shows PM between July 7, 1993, day of year (doy) 200, and end of December 2019, as obtained by the CODE ERP series (Table 1), in a three-dimensional representation. July 7, 2018, thus marks the 25th anniversary of uninterrupted daily CODE (Center for Orbit Determination in Europe) solutions. The date originally motivated our analysis. The ERP series underlying Fig. 1 will be analyzed in detail together with other ERP series in Section 5.

Fig. 1 shows that the pole moves in circles with slowly varying radius around the mean pole. The radius of PM has minima around the years 2000, 2006, and 2012, the maxima lie about halfway between these epochs. The radius of PM reaches the value of about 250 mas in 1996, corresponding to about 8 m on the surface of the Earth. The maximum radius around 2016–17, barely visible, was only about 130 mas, thus about half the size of the 1996 maximum. The minima of the radius were close to zero in the years 2000 and 2006, indicating that the radii of the annual and the Chandler motion were almost the same in these years. The time interval between successive maxima (or minima) of the PM radius represents the beat period of the two fundamental periods of PM, the annual and the Chandler period (Seitz and Müller, 2016).

Principles of our analysis. Following tradition, PM is represented locally by a superposition of the linear motion of the mean pole on the surface of the Earth and of two prograde circular motions, the annual and the Chandler motions. Simple mathematical tools are developed allowing it to extract key long-term characteristics of this model from well-established PM series. The key characteristics of long-term PM are the model parameters, which evolve in time.

We do *not* make the attempt to explain the key characteristics of PM by geophysical models. This may look archaic, as today there are virtually hundreds of papers devoted to the geophysical excitation of PM. There are, however, no long-term observation data available, as geophysical monitoring of the atmosphere and the oceans started only around the middle of the 20th century, much later than the monitoring of PM, where dense and accurate observation series are available, like, e.g., in the IERS C01 IAU2000 series since 1846.

Overview. Section 2 characterizes the analyzed ERP series, Section 3 summarizes key events related to the detection and monitoring of PM and refers to publications relevant in our context. Section 4 defines the models used and specifies the associated parameters. Section 5 discusses the results of analyzing the PM series introduced in Section 2 with the models outlined in Section 4. Section 6 might be considered as an epilogue to our analysis after having presented the method(s) and the key long-term characteristics of PM. Its three subsections provide miscellaneous information related to the methods used here. Section 7 eventually summarizes the key findings, draws conclusions and presents an outlook.

2. Characteristics of the analysed ERP series

The ERP series analyzed subsequently are summarized in Table 1. Column 1 contains the name of the series, column 2 the spacing between consecutive ERP values, column 3 says whether the series is based on one observation technique (ST = single technique) or on a combination of techniques (MT = multi-technique). Column 4 provides additional characteristics. The first three series are analysed in detail, the other ones, after the horizontal separation in Table 1, are ST solutions used for special investigations.

The first of the PM series emerges from the CODE overlapping 3-day solutions, which are described in full detail by Dach et al. (2009, 2015): the CODE ERPs are extracted from the central day of the 3-solutions generated for each calendar day. The x- and y- coordinates of the pole, UT1-UTC, and the corresponding rates are estimated and made available on a daily basis. All daily values refer

Table 1
Characteristics of ERP series analyzed. ST stands for Single Technique, MT for Multi-Technique solutions.

Name	Spcg days	Type	Characteristics
COD	1 d	ST	from GNSS, central day of daily CODE 3-day solutions, 2 PM parms per day (PM positions at day begin and day end), consistent with ITRF in real time, since 1993.6 (doy 200), (Dach et al., 2009)
14 C04	1 d	MT	IERS-generated, combined from VLBI, SLR, GNSS, and DORIS; initially also from astrometry, consistent with ITRF2014, since 1962.0, (Bizouard et al., 2018)
C01	var	ST/MT	IERS-generated, based on IAU 2000, since 1846.0; prior to 1891 spacing of 0.1 years, then 0.05 years; till about 1961 based on astrometry (thus ST), then from IERS 14 C04, thus MT, (Dick and Thaller, 2016, Section 3.5.1)
OA00	≈ 5 d	ST	from astrometry covering interval 1900.0–1992.0, (Vondrák et al., 2000)
OA10	≈ 5 d	ST	from astrometry covering interval 1900.0–1992.0, (Vondrák et al., 2010)
IDS	1 d	ST	based on DORIS, generated by the IDS, 1993.0–2018.0, (Willis et al., 2016; Moreaux et al., 2016)
ILRS	1 d	ST	based on SLR, generated by the ILRS, 1998.0-present (Pearlman et al., 2002)
IVS	var	ST	VLBI solution from IVS, based on 1-day sessions with variable number of sites, available since 1984.0, (Pearlman et al., 2002)
CSR	var	ST	based on SLR, generated by Center for Space Research, since 1976.4
USNO	var	ST	based on VLBI, generated by US Naval Observatory, since 1979.6

to noon GPS time. The time series starts on day 200 of the year 1993 and ends close to real time. The formal errors, which are provided in the CODE series are of the order of 50μ as for the pole coordinates in 1993, ten times smaller at present. For our study of the long-term behavior of the PM series an accuracy of a few mas is sufficient. As the CODE series are overlapping, the correlations in time are in principle an important issue. We are not interested in a time resolution of one to a few days, however. Therefore, correlations in time are not a concern here.

The CODE series is *not* homogeneous, neither from the modeling nor from the data perspectives: frequent model and analysis improvements occurred and a substantial growth of the terrestrial network took place. The resulting improvements for the ERPs are, however, smaller than the required accuracy of pole coordinates. The only serious limitation of the series is its length. This is why the two IERS ERP series, two VLBI- and two SLR-series are included as well in our analysis.

The IERS Annual Report 2015 (Dick and Thaller, 2016, Section 3.5.1), authored by Ch. Bizouard, contains a recent description of the IERS 14 C04 *and* the IERS C01 IAU2000 series regularly published by the IERS Earth Orientation Center located at the *Observatoire de Paris*. Bizouard et al. (2018) provide the most recent description of the IERS C04 series. Both, the C01 and the C04 series are multi-technique (MT) series. Additional important characterizations of the C04- and C01-series are:

- The GNSS observation technique is an essential, if not the dominating contributor to PM in the C04 series since about 1994, when the IGS started its official service.
- From about 1980 to 1994, the VLBI technique was an important, if not the dominating contributor to the IERS 14 C04 series, other contributions stem from satellite Laser ranging (SLR).
- From 1962 to 1980 the C04 series is still mainly based on the astrometric observations analyzed by the ILS (International Latitude Service), later on by the IPMS (International Polar Motion Service), then by the BIH (Bureau International de l'Heure, Paris, France). The C04 series is much longer than the CODE GNSS series, but less homogeneous. The IERS 14 C04 series is fully consistent with the terrestrial reference frame ITRF2014 (Bizouard et al., 2018; Altamimi et al., 2016).
- According to Dick and Thaller (2016, Section 3.5.1), the C01 PM series is composed of contributions from four periods, the first one based on latitude observations from Pulkovo, Greenwich, and Washington, lasting from 1846 to 1899, the second one on optical observations from the ILS from 1900 to 1961, where the analysis (Vondrák, 1999) was used, the third one on IPMS and BIH observations and results from 1962 to 1986, and eventually since 1987 on the IERS combination with observations performed by technique-specific services of the IAG, the International Association of Geodesy.
- Today, the time interval between 1900 and 1961 is in C01 almost uniquely covered by solutions generated in Prague by the team led by Jan Vondrák. As the series play such an important role in the IERS C01 IAU2000 series, the original astrometric series, called OA00 and OA10 (Table 1, series Nos. 4, 5), are included as well in particular for mean PM.
- According to (Bizouard, 2018), PM between 1900.0 and 1962.0 was in essence based on the series OA00 (Vondrak:2000) before December 2018, afterwards on the series OA10 (Vondrak:2010).
- The observations from the time interval 1889–1900 stem from an analysis described by Fedorov et al. (1972), the earlier observations from the analysis documented by Rykhlova (1969).
- The C04 and the C01 time series are regularly updated and end essentially in real time. The starting times were mentioned above, the end times are about one month behind real time for the C04 series. The C01 series is updated regularly as well in intervals of about 18.3 days (1/20 of the year).

The ST series after the horizontal line in Table 1 stem from optical astrometry (OA00, OA10), from the IDS (International DORIS Service) (Willis et al., 2016; Moreaux et al., 2016), the IVS (International VLBI Service for Astrometry and Geodesy) (Nothnagel et al., 2017), and the ILRS (International Laser Ranging Service) (Pearlman et al., 2002). The "oldest" SLR solution from the Center for Space Research in Texas and the "oldest" VLBI solution from the US Naval Observatory are included as well. All series are available through the IERS,[3] where short descriptions may be found as well.

According to the *Product table* in the IDS homepage[4] the DORIS PM series are based on the combination of the results of the DORIS Analysis Centers and are made available "occasionally", e.g., through the Crustal Dynamics Data Information System (CDDIS). Table 2 characterizes the DORIS PM series used subsequently. The first two entries, ids18wd01 and ids19wd01, are original IDS PM series. The first of these series is also provided under the IERS-link provided in footNote 3. The third entry in Table 2 is an excerpt of ids19wd01, disregarding the PM positions prior to day 200 of the year 1993.

Simulated PM series may be analyzed as well with our standard analysis tool. An example will be provided in Section 6.3.

3. Previous analyses

The phenomenon of PM was postulated in the 18th century by Leonhard Euler based on theoretical studies about the rotation of solid bodies (Euler, 1766). Since then,

[3] http://hpiers.obspm.fr/eop-pc/index.php?index=analysis&lang=en.
[4] https://ids-doris.org/ids/data-products/tables-of-data-products.html.

Table 2
DORIS PM series made available by the IDS and used in our analysis; all solutions are aligned to ITRF14.

Solution	time interval	Availability/ Remarks
ids18wd01	1993.0–2018.0	http://hpiers.obspm.fr/eop-pc/index.php?index=analysis&lang=en or ftp://cddis.gsfc.nasa.gov/doris/products/eop/
ids19wd01	1993.0–2019.5	available under ftp://cddis.gsfc.nasa.gov/doris/products/eop/
ids19wd01-s	1993.6–2019.5	same as ids19wd01, but starting at 1993.6

astronomers were searching for observational evidence of PM for more than a century. Friedrich Küstner was eventually credited with PM detection based on his work (Küstner, 1888). The early history of PM is, however, much more complex – Verdun and Beutler (2000) provide a concise summary of the essential facts.

In a series of four articles (Chandler, 1891a,b, 1892a,b), all published in the Astronomical Journal in the years 1891 and 1892, Seth Carlo Chandler postulated that PM is composed of two parts, the annual component with a period of 365.25 days and a component with a period of about 14 month, replacing the 10 month period predicted by Euler. He provided estimates of the amplitudes and phases for both constituents based in essence on all observations made in the 19th century. In his honor the 14-month period is called the Chandler period, the corresponding constituent of PM the Chandler motion.

In 1901 Chandler (1901) published one more article in the Astronomical Journal, where he claimed that the 14-month constituent consisted of two components, separated in period by about eight days, explains the strong variation of the amplitude of Chandler motion. As opposed to his articles of 1891 and 1892, Chandler (1901) did not get the same attention in the subsequent decades. Chandler's article of 1901 is discussed at length in the detailed history of the detection of PM by Carter and Carter (2000), which perhaps saved Chandler's 1901-hypothesis from oblivion. We will provide evidence in SubSection 5.2 that Chandler's hypothesis might be right.

Küstner's and Chandler's works were pivotal for the establishment of the ILS in 1899. The ILS was dedicated to the monitoring of PM by initially five latitude observatories at a Northern latitude of about 39.8°.

In his most influential article (Jeffreys, 1940) Sir Harald Jeffreys analyzed ILS PM values with a spacing of 0.1 years (36.5 days) from 1892 to 1938. His treatment was based on the assumption that PM "consists of a free nutation of the Earth's axis about a principal axis, with a period of about 14 months . . .and a superposed annual motion in an ellipse, . . .". The model was thus based on Chandler's publications of 1891 and 1892. The Chandler period was assumed to be constant and its length was estimated by Jeffreys. Jeffreys' analyses thus ignored the article (Chandler, 1901).

Jeffreys first determined a model for the annual periodic motion from the ILS data set, then subtracted this model from the observed PM data, to eventually approximate the solution of the Liouville-Euler equations (Beutler, 2005, Vol. 2, Chapter 2) using the reduced PM series. His version of the Liouville-Euler equations contained a friction term, which is responsible for damping of the amplitude of Chandler motion. A motion of the mean pole was no issue at that time. Jeffreys' method was also dictated by the limited computing power at that time. His method was modified much later, e.g., by Vicente and Wilson (2005), with the goal to define a new international origin of the Earth's pole.

We will use one element of the Jeffreys analysis, namely to subtract the annual PM from the observed PM, to analyze the difference with our so-called alternative model (Section 5.2). As mean PM cannot be ignored nowadays, mean PM had to be subtracted as well before analyzing the remaining Chandler part of PM.

Three articles by scientists in the former Soviet Union should be mentioned. Two of them were published in English in the journal "Soviet Astronomy", one in the IAU (IAU = International Astronomical Union) Symposia series: Fedorov et al. (1972) describe the determination of the Earth's pole from 1890 to 1969 using 92 astrometrical observation series from 72 observatories. Rykhlova (1969) describes the PM series 1846.0–1891.5 derived from the latitude observations of the Pulkovo, Greenwich, and Washington observatories. The 19th century part of the C01 PM series in Table 1 stems from these Russian analyses.

Fedorov and Yatskiv (1965) interpret these PM series and describe in particular an apparent bifurcation of the Chandler period, which would in essence take up the idea of Chandler's hypothesis stated by Chandler (1901). Fedorov and Yatskiv (1965) of course did not have the C01 series available for their analysis, but had to use older PM series. Malkin and Miller (2011) follow the tradition of the early Russian investigations. Their analysis of the entire C01 PM series suggests the existence of two more major phase changes of the Chandler wobble in addition to that around 1920–1930 and near the boundaries of the C01 time series, which are all accompanied by small amplitudes.

As opposed to the findings of the Soviet scientists Bernard Guinot (1925–2017) stated that "no evidence was found for a double Chandlerian period, nor for a correlation between amplitude and period" (Guinot, 1972). The PM information available to Bernard Guinot was, of course, much shorter than today's IERS C01 IAU 2000 series and not comparable in quality. He used latitude observations from twenty stations in the time interval 1900–1971.

Vondrák et al. (1995) derive PM, UT1-UTC[5] and celestial pole offsets at five-day intervals from astrometrically

[5] Actually UT1-TA1, where TA1 is atomic time.

observed latitudes of 19 observatories, including the sites of the ILS. The time series spans the time period from 1900 to 1992.0. Various versions of Vondrák's analysis are the basis for the C01 in the first sixty years of the 20th century: the C01 pole positions from 1900 to 1961 are in essence taken over from this reference. The solutions presented by Vondrák et al. (1995) were not yet considered as final, because the Hipparcos star catalogue, based on the results of the ESA mission with the same name, became available only later. Vondrák (1999), covering the time interval 1899.7–1992.0, contains the updated results. Using a special technique called "convoluting the PM series with a window with a width of 8.5 years", Vondrák (1999) estimates the time evolution of mean PM and the parameters of the Chandler and annual motions. The astrometry series used in the IERS C01 IAU2000 series are described in detail by Vondrák et al. (2000, 2010).

Gross and Vondrák (1999) compare polar wander (mean PM) derived from astrometry and from space geodetic methods, Gross (2007) reviews the long-term aspects of Earth rotation and monitoring in a very broad sense. In the latter reference one finds a description of the relevant observation techniques, from lunar occultations to today's space geodetic techniques.

Schuh et al. (2001) analyze PM as represented by the C01 series and by the re-analysis performed and described by (Vondrák et al., 1995; Vondrák, 1999). The authors define a numerical model for PM, which may be seen as a building block of our model outlined in Section 4. The (Schuh et al., 2001)-model in essence consists of one constant linear motion for each mean pole coordinate, and one cosine function, characterized by amplitude and phase, to model the annual and the Chandler motions. As different amplitudes and phases are determined for the x- and the y-coordinates of the pole, the model *de facto* contains one pro- and one retrograde wave for the annual and for the Chandler constituent. The procedure shares an important characteristic with our method: all model parameters are determined in one least-squares parameter estimation process.

Höpfner (2004) analyzed five long-term PM series around 2003 including the best version of the IERS C01 series available at that time, the astrometric series OA00, and the series SPACE2001 based on space-geodic observations starting in 1976. The analysis includes the PM components and the derived angular momentum data. As all series ended between 1992 and 2002 the effects we are particularly interested in, the substantial change of mean PM starting around the end of the 20th century and the new minimum of the radius of the Chandler motion around 2018, were not accessible to the analysis completed in 2003.

Vondrák and Ron (2005) analyzed "the great Chandler wobble change in 1923–1940" using the best astrometric PM series available in 2004. They use the technique proposed by (Vondrák, 1999) to represent the long-term evolution of PM and they proposed various excitation mechanisms to explain PM in the mentioned time interval. As Guinot (1972), Vondrák and Ron (2005) rule out a variable or a double Chandler period and present instead several mechanisms to explain the great Chandler wobble change 1923–1940.

McCarthy and Seidelmann (2009, Section 5.2.2.3) write that the amplitude of the Chandler motion is "known to be variable, but of the order of 150 mas" and that "annual PM is a stable prograde motion with an amplitude of about 90 mas". McCarthy and Seidelmann (2009, Chapter 4) also describe the known variations of Earth rotation, in particular the variations of the "clock" Earth w.r.t. a better clock, realized by atomic time, ephemeris time, and lunar eclipses, at different epochs.

Roy and Pelletier (2011) analyzed a PM series derived from space-geodetic data (SPACE2008) between 1976 and 2009 generated by the Jet Propulsion Laboratory (JPL). The authors document a substantial change of mean PM around 1992 (Roy and Pelletier, 2011, Fig. 1). Their method is different to what was done here: the observed PM series was filtered with a so-called Butterworth filter, then the filtered series was approximated by independent linear functions of time in the intervals 1976–1992 and 1992–2009. No continuity condition was imposed in 1992.

Chen et al. (2013) analyzed among other the C04 series of PM and describe "...around 2005 ...an abrupt departure (of the mean pole) from the drift direction seen over the past century". We believe that the authors describe in essence the same phenomenon as we, but their time tag differs by about ten years from ours. The issue will be discussed in detail in Section 5.1.

Wahr et al. (2015) studied the impact of mean PM on the mean pole tide and on the GRACE-derived results for the harmonics C_{21} and S_{21} of the Earth's gravity field. Wahr et al. (2015, Fig. 1) show that mean PM as derived from global isostatic adjustment (GIA) and mean PM derived from the IERS series were tracking each other quite well until about the year 2000. Afterwards, the mean IERS pole positions leave the GIA prediction. The sharp bend in mean PM, which is assigned to the year 2000 by Wahr et al. (2015) will be discussed in Section 5.1.

Seitz and Müller (2016) quote similar orders of magnitude for PM as McCarthy and Seidelmann (2009), also pointing out that the Chandler amplitude is subject to strong variations in time. The review article is in essence based on Seitz and Schmidt (2005), who applied a dynamic Earth system model and wavelet techniques to the IERS C01 series. Seitz and Schmidt (2005, Fig. 1) show that the Chandler amplitude varies, according to their study, between 0 mas, e.g., in the 1920s, and about 250 mas, e.g., in the 1950s. The same figure also shows that the Chandler amplitude is decreasing from a value of about 150 mas to about 100 mas when approaching the year 2000, the last data point in the (Seitz and Schmidt, 2005)-analysis. The wavelet techniques also allowed it to see slow variations in the Chandler period.

In Section 1 we stated that it is not our goal to model PM by solving the equations of motion of the Earth as a

function of the astronomical and geophysical torques acting on it. This modeling process is of course extremely important to truly understand the structure and the rotational motion of the Earth as a planet consisting of a non-rigid solid body, of the atmosphere and the oceans. Today, Earth rotation is an interdisciplinary branch of science involving astronomy and geophysics including meteorology. Two fundamental books and one article, all published in the second half of the 20th century, must be mentioned in this context. The book (Munk and McDonald, 1960) was published in 1960. Remarkably, it was dedicated to Sir Harold Jeffreys. According to the authors the book "is an account of certain irregularities in the rotation of the Earth which are not ordinarily included in the gravitational theory" – a clear understatement. The monograph (Lambeck, 1980) was first published in 1980, twenty years after (Munk and McDonald, 1960). Lambeck (1980) writes in the preface "Munck and McDonald thoroughly reviewed the subject [of Earth rotation] . . .and it is unusual to find any aspect of the problem that they have not touched upon." He then lists important developments since 1960, including the use of atomic time in Earth rotation monitoring, much better geophysical knowledge of the Earth's interior, improved interpretation of ancient eclipse data, developments in space science, in particular satellite geodesy [at the time mainly based on SLR], and VLBI. The emphasis of the book is on the geophysical discussion. The article (Barnes et al., 1983) describes in great detail the relationship between the monitored atmosphere angular momentum functions (AAM) and the measured geodetic & astronomical counterparts. Their formulation of the Liouville-Euler equations is still used today for describing the rotation of a non-rigid Earth surrounded by atmosphere and oceans. The article allowed it to "easily" model PM and LoD as a function of the geophysical models – at least where torques with quasi-periods of one to several years are concerned. It became in particular feasible to use the AAM time series from meteorological monitoring for Earth rotation monitoring. With time evolving, Oceanic Angular Momentum (OAM) and Hydrological Angular Momentum (HAM) were monitored and used in the modeling process as well. The monitoring of these geophysical angular momentum series are today coordinated and made available through the IERS. The impact of the above pioneer work is also documented by the dedicated workshop (Plag et al., 2005).

Let us conclude this excursion into the "modeling branch" of Earth rotation by mentioning a few recent publications. The diminishment of the Chandler amplitude in the first decade of the 21th century was also analyzed by Bizouard et al. (2011), who directly integrated the Liouville-Euler Equations in the time interval 1949.5–2009.5 using the atmospheric and oceanic angular momentum functions (AAM and OAM) to obtain PM time series. Zotov and Bizouard (2012) derive the Chandler wobble excitation (right-hand sides of the Liouville-Euler equations) from PM observations by using a special kind of filtering. The work was continued and extended; it is illustrated by Zotov et al. (2019) and eventually resulted in a doctoral thesis (Zotov, 2019). The monograph (Bizouard, 2020), to be published later this year, contains among many other aspects the most recent modeling results. Ron et al. (2019) integrated a generalized version of the Liouville-Euler equations based on the formulation (Brzezinski, 1994) to model PM from 1980.0–2018.5 using different kinds of angular momentum functions; so-called geomagnetic jerks were taken into account as well.

4. Modeling polar motion

Deterministic model for short PM series. For time intervals of up to, let us say, 4–5 years, PM may be described as the superposition of a fixed mean pole position and two prograde circular motions around the mean position, with periods of one year (annual motion) and of about 14 months (Chandler motion). Let $l(t)$ and $m(t)$ be the PM components and $\bar{l}, \bar{m}$ the mean pole coordinates. The annual constituent is assumed to have a period of $P_y \doteq 365.25$ days, the Chandler motion one of $P_C = 432.2485 \approx 432.25$ days; ω_y and ω_C are the corresponding angular velocities. The annual period is an approximation of the tropical year, the adopted value for the Chandler period is that used by Vondrák (1999), within the formal error bars of the value recommended by Gross, 2007, Table 11. The Chandler PM over short time intervals may thus be written as:

$$\begin{aligned} l(t) &= \bar{l} + \rho_y \cos(\omega_y t + \phi_{y0}) + \rho_C \cos(\omega_C t + \phi_{C0}) \\ m(t) &= \bar{m} + \rho_y \sin(\omega_y t + \phi_{y0}) + \rho_C \sin(\omega_C t + \phi_{C0}) \end{aligned}$$

$$\begin{aligned} l(t) &= \bar{l} + \rho_y \cos\phi_{y0} \cos\omega_y t - \rho_y \sin\phi_{y0} \sin\omega_y t \\ &\quad + \rho_C \cos\phi_{C0} \cos\omega_C t - \rho_C \sin\phi_{C0} \sin\omega_C t \\ m(t) &= \bar{m} + \rho_y \sin\phi_{y0} \cos\omega_y t + \rho_y \cos\phi_{y0} \sin\omega_y t \\ &\quad + \rho_C \sin\phi_{C0} \cos\omega_C t + \rho_C \cos\phi_{C0} \sin\omega_C t \end{aligned} \quad . \tag{1}$$

The first two of Eq. (1) represent the circular motions by their (constant) amplitudes and the phase angles referring to the time origin. The time origin $t = 0$ is subsequently associated with January 1, 2000, 0^h UT.

The second pair of Eq. (1) is easily obtained from the first pair by applying the trigonometric theorems

$$\begin{aligned} \cos(\alpha + \beta) &= \cos\alpha\cos\beta - \sin\alpha\sin\beta \\ \sin(\alpha + \beta) &= \sin\alpha\cos\beta + \cos\alpha\sin\beta \end{aligned} \tag{2}$$

on the right-hand sides, with $\alpha = \phi_{..0}$ and $\beta = \omega_{..} t$.

At first sight the second pair of Eq. (1) is more complicated than the first one. The second pair has, however, the decisive advantage that the PM components $l(t)$ and $m(t)$ are linear functions of the *initial annual components* $l_{y0} \doteq \rho_y \cos\phi_{y0}, m_{y0} \doteq \rho_y \sin\phi_{y0}$, and of the *initial Chandler*

components $l_{C0} \doteq \rho_C \cos\phi_{C0}, m_{C0} \doteq \rho_C \sin\phi_{C0}$. Eq. (1) may thus be given the following simple form:

$$\begin{aligned} l(t) &= \bar{l} + l_{y0}\cos\omega_y t - m_{y0}\sin\omega_y t \\ &\quad + l_{C0}\cos\omega_C t - m_{C0}\sin\omega_C t \\ m(t) &= \bar{m} + m_{y0}\cos\omega_y t + l_{y0}\sin\omega_y t \\ &\quad + m_{C0}\cos\omega_C t + l_{C0}\sin\omega_C t \end{aligned} . \tag{3}$$

The total number of parameters in Eq. (3) is $n_p = 6$. The parameters are the two mean pole coordinates $\bar{l}, \bar{m}$, the two initial annual components l_{y0}, m_{y0}, and the two initial Chandler components l_{C0}, m_{C0}. Eq. (3) are linear in all six parameters.

Eqs. (4) in (Vondrák, 1999) are closely related to Eq. (3), but include in addition retrograde annual and Chandler terms, and the rates of the mean PM components. Vondrák (1999) used these equations to study the long-term evolution of the parameters in these equations, by applying them to their astrometric PM series, using a sliding window of 8.5 years; one solution was generated for each window. In this way a filtered PM series was obtained covering the same time interval as that of the original series. Eq. (3) of course might be used in the same way. We make, however, different use of them.

Deterministic model for long time intervals. Assuming a fixed position of the mean pole and constant initial components for the two circular motions is not flexible enough when analyzing long PM time series. Flexibility may, e.g., be achieved by assuming the parameters in Eq. (3) not as constants, but as slowly varying functions, parameter functions, of time:

$$\begin{aligned} l(t) &= \bar{l}(t) + l_{y0}(t)\cos\omega_y t - m_{y0}(t)\sin\omega_y t \\ &\quad + l_{C0}(t)\cos\omega_C t - m_{C0}(t)\sin\omega_C t \\ m(t) &= \bar{m}(t) + m_{y0}(t)\cos\omega_y t + l_{y0}(t)\sin\omega_y t \\ &\quad + m_{C0}(t)\cos\omega_C t + l_{C0}(t)\sin\omega_C t \end{aligned} . \tag{4}$$

$l_{y0}(t)$ and $m_{y0}(t)$ are called *initial annual component functions* subsequently, $l_{C0}(t)$ and $m_{C0}(t)$ *initial Chandler component functions*. The six parameter functions in Eq. (4) are defined as piecewise linear and continuous functions, which preserve the linearity of the parameter estimation problem.

Let T_B and T_E mark the start and the end of the ERP series under investigation. Let the interval $I = [T_B, T_E]$ be divided into n_s subintervals of the same length $\Delta t \doteq \frac{T_E - T_B}{n_s}$. The $n_s + 1$ subinterval boundaries are thus $t_i \doteq T_B + i\Delta t, i = 0, 1, \ldots, n_s$. The parameter functions within the subinterval $I_i = [t_{i-1}, t_i], i \in (1, 2, \ldots, n_s)$ of length $\Delta t = t_i - t_{i-1}$, i.e., $t \in I_i$ are defined as the following piecewise linear and continuous functions:

$$\begin{aligned} \bar{l}(t) &= \tfrac{(t_i - t)\bar{l}_{i-1} + (t - t_{i-1})\bar{l}_i}{\Delta t} \\ \bar{m}(t) &= \tfrac{(t_i - t)\bar{m}_{i-1} + (t - t_{i-1})\bar{m}_i}{\Delta t} \\ l_{y0}(t) &= \tfrac{(t_i - t)l_{y0,i-1} + (t - t_{i-1})l_{y0,i}}{\Delta t} \\ m_{y0}(t) &= \tfrac{(t_i - t)m_{y0,i-1} + (t - t_{i-1})m_{y0,i}}{\Delta t} \\ l_{C0}(t) &= \tfrac{(t_i - t)l_{C0,i-1} + (t - t_{i-1})l_{C0,i}}{\Delta t} \\ m_{C0}(t) &= \tfrac{(t_i - t)m_{C0,i-1} + (t - t_{i-1})m_{C0,i}}{\Delta t} \end{aligned} \tag{5}$$

The function values $\bar{l}_i$ and $\bar{m}_i$ are the mean pole coordinates at the subinterval boundaries, the values $l_{y0,i}, m_{y0,i}$ are the initial annual PM components at the subinterval boundaries, the values $l_{C0,i}, m_{C0,i}, i = 0, 1, \ldots, n_s$ the initial Chandler components at the suinterval boundaries. They are the parameters of the model (4). Inserting Eq. (5) into Eq. (4) tells that the resulting PM model is linear in all its parameters. Instead of six parameters as in Eq. (3), there are now $n_p = (n_s + 1) \cdot 6$ parameters in the model (4), (5) – indicating that the new model is much more flexible than the model (4), which is based on one mean pole position, and on constant initial annual and Chandler components.

Different numbers of subintervals might be used for the parameter functions of the mean, the Chandler, and the annual motion. Our implementation actually offers this option, but no use will be made of it subsequently.

The model (4), (5) promises sound performance, if the length Δt of the subintervals is large compared to the two basic periods of PM, the annual and the Chandler periods. For smaller values of Δt the correlations between the estimated parameters $l_{y0,\ldots}, m_{y0,\ldots}$ on the one hand and $l_{C0,\ldots}, m_{C0,\ldots}$ on the other hand become significant. A typical value for the subinterval length is therefore $\Delta t \approx 6.45$ years, corresponding to the beat period of the annual and the Chandler period. An erratic behavior of the parameters of a particular type must be expected, however, if Δt is of the order of the annual and Chandler periods or even smaller. This behavior can be removed either by reducing the number n_s of subintervals, where one would end up with the typical subinterval lengths mentioned, or by providing additional information to the adjustment process.

Filtered parameter series. Subsequent parameter values of the same parameter function (5) may be filtered directly in the adjustment process. This is done by constraining the change of subsequent parameter values or, more generally, of linear combinations of subsequent parameter values of the same parameter function. Constraining the change of subsequent parameter values of the same parameter function would constrain the mean linear motion over the entire time interval, which is not intended. Therefore, we constrain the temporal changes between subsequent parameter differences, which is equivalent to constraining the second time derivatives of the parameter functions.

Let us use the parameters $\bar{l}_i, i = 1, 2, \ldots, n_s$ of mean PM to outline the technique: the constraints request that the differences between subsequent mean PM differences are zero. A weight w is associated with these equations.

$$\begin{aligned}(\bar{l}_{i+2}-\bar{l}_{i+1})-(\bar{l}_{i+1}-\bar{l}_i) &= 0\\ \bar{l}_{i+2}-2\bar{l}_{i+1}+\bar{l}_i &= 0\end{aligned} \qquad i=0,1,\ldots,n_s-2. \tag{6}$$

Eqs. (6) may be viewed as additional linear observation equations taking into account a priori knowledge. They are rather special, as they are error-free. We call them *pseudo-observation equations* and write them in matrix form:

$$\boldsymbol{L}\bar{\boldsymbol{l}}=\boldsymbol{0}, \tag{7}$$

where

$$\begin{aligned}\boldsymbol{L} &= \begin{pmatrix} 1 & -2 & 1 & \ldots & \ldots & \ldots & 0 & 0 & 0\\ 0 & 1 & -2 & 1 & \ldots & \ldots & 0 & 0 & 0\\ \ldots & \ldots & \ldots & \ldots & \ldots & \ldots & \ldots & \ldots & \ldots\\ \ldots & \ldots & \ldots & \ldots & \ldots & \ldots & \ldots & \ldots & \ldots\\ \ldots & \ldots & \ldots & \ldots & \ldots & \ldots & \ldots & \ldots & \ldots\\ 0 & 0 & 0 & 0 & 0 & 1 & -2 & 1 & 0\\ 0 & 0 & 0 & 0 & 0 & 0 & 1 & -2 & 1 \end{pmatrix}\\ \bar{\boldsymbol{l}}^T &= (\bar{l}_0,\bar{l}_1,\ldots,\bar{l}_{n_s})\\ \boldsymbol{0}^T &= (0,0,\ldots,0).\end{aligned} \tag{8}$$

The matrix $\boldsymbol{L}$ has n_s+1 columns and n_s-1 rows. The number n_s of subintervals can be made much larger when adding the constraints (7) than in the standard case without these constraints, represented "only" by Eqs. (4) and (5).

The Eq. (7) related to the second differences of the mean PM components $\bar{l}_i, i=0,1,\ldots,n_s$ can easily be transformed into the corresponding normal equation (NEQ) constituent:

$$w\boldsymbol{L}^T\boldsymbol{L}\bar{\boldsymbol{l}}=\boldsymbol{0}, \tag{9}$$

where w is the weight associated with these equations. The NEQ constituent is simply superimposed to the NEQ system emerging from the observation Eqs. (4), (5). The resulting NEQ system is exactly that of the Tikhonov regularization (Press et al., 1996, *linear regularization methods*).

Defining meaningful weights w for the constraints (pseudo-observation equations) is not trivial. Press et al. (1996) recommend to set an initial weight by asking the trace of the normal equations referring to the actual observations to equal the trace of the normal equations stemming from the pseudo-observations (constraints), and then to refine the weight by trial and error, a procedure which truly is a *numerical recipe*. We define the weight w based on known characteristics of mean PM as, e.g., emerging from the use of the purely deterministic model with a "modest" spacing. For the parameter type $\bar{l}$ we put:

$$w=f_s\left(\frac{f\sigma_o}{\dot{\bar{l}}\Delta t}\right)^2. \tag{10}$$

f_s is the factor taking into account the sampling of the PM observation series: when analyzing, e.g., the CODE GNSS or the C04 series with a 1-day spacing between subsequent PM values, $f_s=1$, when analyzing the C01 series, with a spacing of 1/10 y or 36.5 days, $f_s=1/36.5$. σ_0 is the standard deviation of the residuals of the PM values (about 14 mas for space-geodetic series, about 40 mas for the historic C01 series), $\dot{\bar{l}}$ represents the mean annual PM rate for both mean PM coordinates, and f^2 is the scaling factor of the weight. 1/f is thus the scale factor for the standard deviation of the constraints (pseudo-observations); for $f=0$ one obtains the free or unconstrained motion, for $f\to\infty$ a linear motion on a straight line with constant rate. We use the value

$$\dot{\bar{l}}\doteq 3\ \text{mas/y} \tag{11}$$

as mean PM rate for the mean PM coordinate $\bar{l}$.

The same regularization is applied independently to all six parameter types (5). The value $\dot{\bar{l}}$ in Eqs. (10), (11) has to be replaced by the mean rates of the other five parameter functions. It turned out that the numerical value of 3 mas/y can be used for all six parameter functions.

Summary. The model (4), (5) for PM results in a linear parameter estimation procedure. The length of the subinterval is of the order of the beat period of the annual and Chandler periods, i.e., about 6.45 years. The subinterval length may be reduced substantially, if the defining parameters are filtered according to Eqs. (7), (10). The parameters referring to mean PM and to the periodic constituents are determined in one and the same parameter estimation procedure. The resulting parameters are thus mutually consistent.

5. Results

Fig. 2 give an impression of the approximation quality achieved with the model (4), (5)[6] using a spacing of about 6.45 years, the beat period of the annual and Chandler periods, when applied to the first three ERP series of Table 1. The subinterval lengths are only approximately the same in the three figures, because the number of subintervals is an integer number in the three cases. The figures show the PM values as a function of time (solid red & blue lines for the x- and y-coordinates, respectively), and the residuals "observations-model" as dash-dotted lines. The number n_s of subintervals, the total number of parameters, and the standard deviations of the residuals, are provided in the title of each of the series.

Fig. 2 (left, center) indicate that the fit is roughly of the same quality when analyzing the CODE GNSS and the C04 series, which is (mostly) based on modern space techniques. The residuals in Fig. 2 (right) are clearly larger in the interval 1891–1961 than in the interval 1962–2019, they

[6] the corrected series was used, explained later in the section.

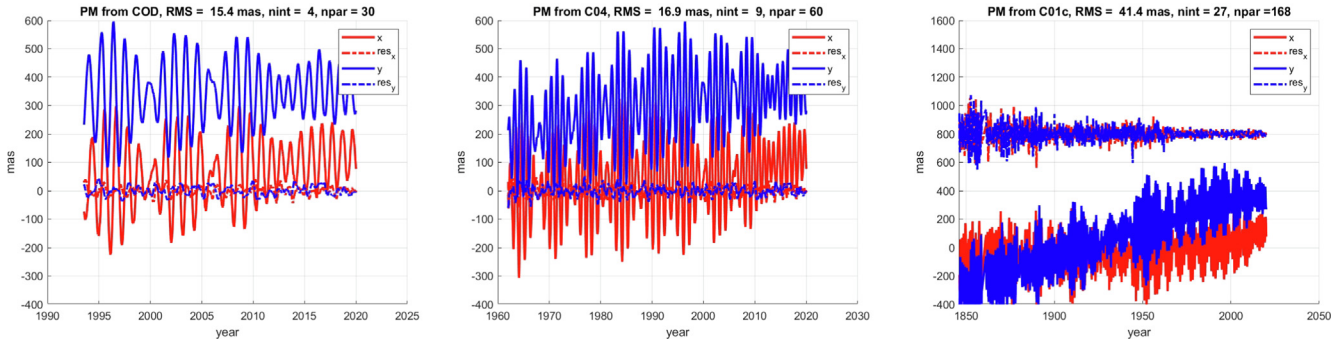

Fig. 2. Polar motion in mas and residuals of fit. Left: from CODE overlapping 3-day solutions from 1993, doy 200 to the end of 2019, center: from IERS 14 C04, 1962.0 to 2020.0, right: from IERS C01, 1846 to the end of 2019, residuals offset by 800 mas.

are even larger prior to about 1891. The well-known data gap between November 1858 and November 1860 can be seen as well. The residuals in Fig. 2 (right) witness the composite nature of the C01 series.

Mean PM is analyzed in Section 5.1, the annual and the Chandler motions in Section 5.2. The treatment follows the same pattern within the subsections: the results based on the CODE GNSS are discussed first (CODE series from Table 1), then the results from the other space techniques, namely SLR, VLBI, DORIS, and of the IERS 14 C04 series, combining the results of all space-geodetic techniques. The corresponding series of Table 1 are used for this purpose. The oldest of the available ST space-geodetic series starts in 1976, the C04 series starts even in 1962. Eventually, the series IERS IAU2000 C01, starting in 1846, is analyzed. As the C01 series is based on the pure astrometric series prior to 1962, the two series OA00 and OA10 (Table 1) covering the time interval 1900–1961, are included in the discussion as well.

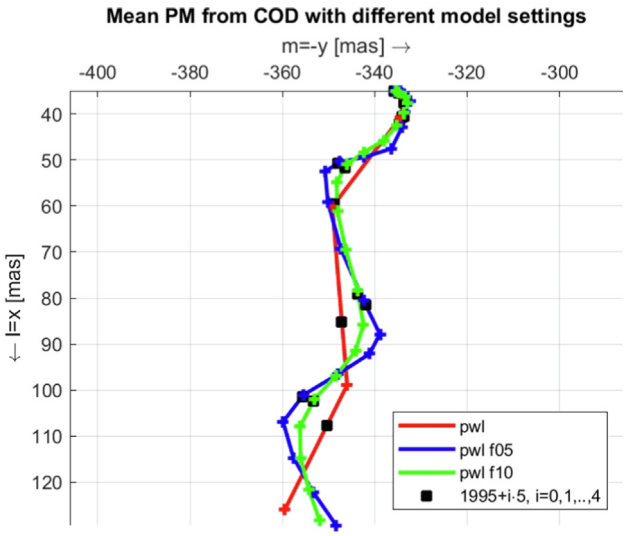

Fig. 3. Mean PM in mas resulting from CODE series (Table 1) based on model (4), (5) with $n_s = 4$ subintervals (red), with $n_s = 20$ subintervals and filtering according to Eqs. (6), (10) with $f = 5$ (blue) and $f = 10$ (green); pwl stands for piecewise linear; the black squares are time stamps on the mean PM trajectories at 1995.0, 2000.0, 2005.0, 2010.0, 2015.0 (from top to bottom). (For interpretation of the references to color in this figure legend, the reader is referred to the web version of this article.)

5.1. Mean polar motion

Mean PM based on CODE 3-day solution. The red curve in Fig. 3 shows mean PM resulting from the CODE ERP series based on the purely deterministic model (4), (5) with $n_s = 4$ subintervals with a length of $26.4/4 \approx 6.6$ years. The blue and green curves result from analyzing the same PM series, but they are both based on a finer spacing with $n_s = 20$ subintervals (corresponding to a subinterval length of about 1.3 years) and on the filter approach: the crosses "+" on the curves represent the filtered mean PM positions using Eqs. (6), (10). The blue curve corresponds to $f = 5$, the green curve to $f = 10$ in Eq. (10). The five black squares on each trajectory mark the mean pole positions at five year intervals from 1995 to 2015, from top to bottom. The results are consistent in the sense that on the average mean PM follows roughly the meridian at Western longitude of $\lambda \approx 13^\circ \ldots 15^\circ$ for the entire time interval of 26 + years. According to the model mean PM was substantially slower around 1993 than it is at present. The direction of the motion differs substantially from the value of 79.2° West reported by Gross (2007), the well-established direction of mean PM for the entire 20th century.

All CODE curves show an increasing rate of all mean PM coordinates since 1993.6. This is also illustrated by the black squares on the mean PM curves. From now on, our analysis will be based on the filtered approach using Eqs. (6), (10) with $f = 10$ and 20 subintervals. The smoothing factor is somewhat arbitrary. It makes the attempt to minimize spurious excursions.

Fig. 4 shows mean PM according to model 4, 5, 6, 10 with $n_s = 20$ subintervals, and $f = 10$, with different end epochs. The figure illustrates how PM has looked like "in real time" in the time interval 1993.6–2020.0. Let us look in particular at the dash-dot red curve with the end epoch 2011: Even with $f = 10$ the curve looks more or less linear after 2005. The sharp bend around 2010 becomes obvious only when including data till 2015.0 or later. An analyst around 2012 thus must have got the impression that a

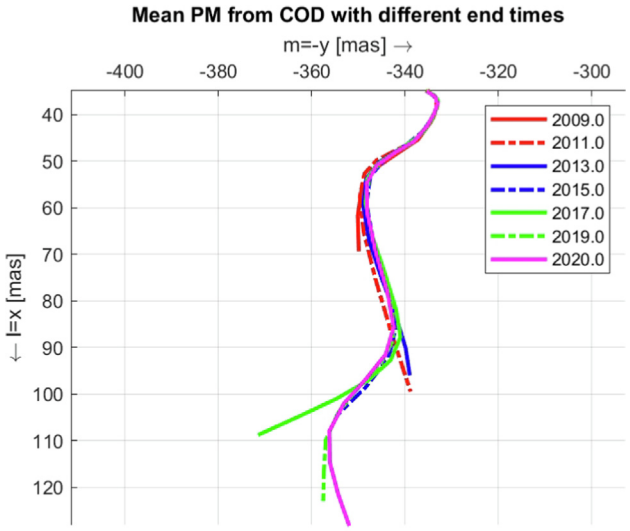

Fig. 4. Mean PM in mas from CODE series (Table 1) based on model (4), (5) with subintervals of approximative length 1.3 years and filtering according to Eqs. (6), (10) with $f = 10$ using different end epochs.

sharp bend took place in the mean PM curve around 2005.0 and that mean PM followed a straight line along a meridian of about 15–20° East afterwards.

As opposed to that, mean PM according to the CODE solution follows a sinuous line since 1993.6 when using data till 2020.0. The deviations from a straight line get smaller, when the smoothing factor f increases – which is expected. The red and the blue curves in Fig. 3 show longer time intervals of a more or less straight line PM, followed by "sharp bends" in relatively short time intervals. In the purely deterministic model (red) this behavior is implemented by design.

The effect of regularization may be checked by the correlation matrix related to the parameters of a particular type. The correlation coefficients of mean PM positions drop from 1 on the diagonal to below 0.1 after (before) 4–5 subintervals, corresponding to 5–6 years. This general result also holds for the initial components of the annual and the Chandler components. The correlation matrix is well suited to fine-tune the scaling factor f in Eq. (10).

Mean PM based on space-geodetic and IERS C04 solution. Fig. 5 (top) shows mean PM as obtained with model 4, 5, 6, 10, $f = 10$, when analyzing the single-technique (ST) PM series of Table 1 and the combined IERS 14 C04 series. After about 1996 all estimated mean PM curves are consistent with the CODE GNSS curve. The direction of mean PM after 1993 therefore *cannot be* a GNSS or CODE artifact. With the exception of the ILRS solution, which only starts around 1998.0[7] and the DORIS solution ids18wd01 starting in 1993.0, all other mean PM solutions are based on PM series starting much earlier than the CODE GNSS and the DORIS solutions. They consistently follow an almost East to West path between 1980 and 1993,

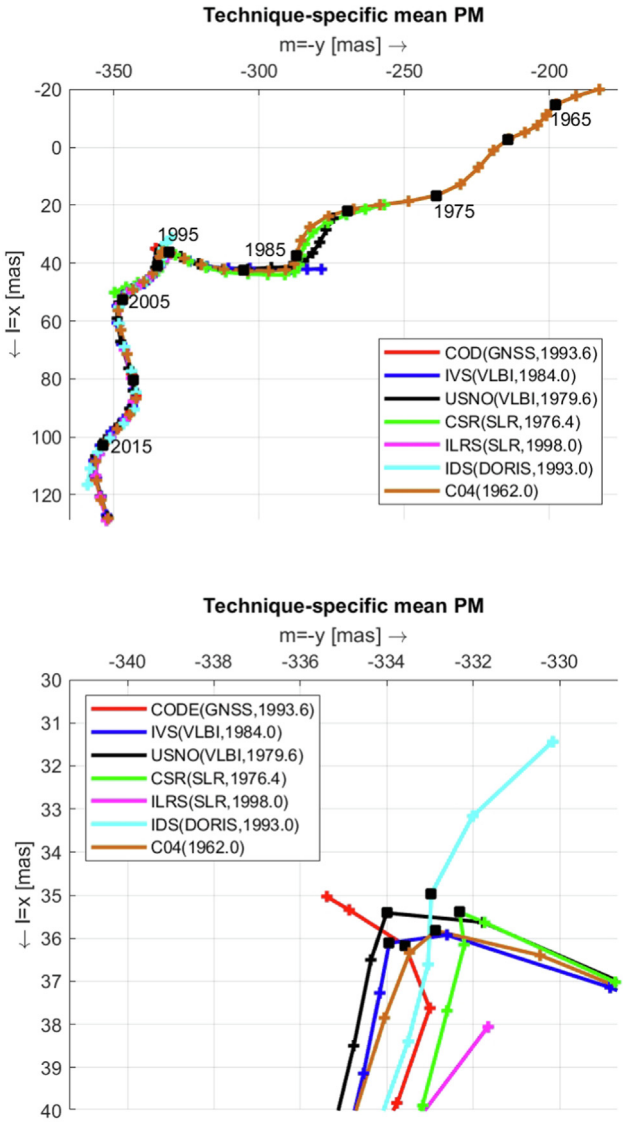

Fig. 5. Top: Mean PM in mas resulting from CODE GNSS, VLBI (two sols), SLR (two sols), and DORIS between 1976.4 and present; IERS 14 C04 series included for reference; the black squares in the top figure are time stamps on the mean PM trajectory from C04 between 1965 and 2015 at a spacing of five years; bottom: PM around the sharp bend of direction; the black squares mark the closest boundary epochs of the individual mean PM curves to 1996.0.

to switch to a West by South-West trajectory prior to 1980, which corresponds to the mean PM value reported by Gross (2007). Fig. 5 (top) shows for all early space-geodetic ERP series, which are based on VLBI or SLR, a sharp bend around 1994–1997.

Fig. 5 (bottom) provides a zoom of Fig. 5 (top) and allows a detailed view of all space-geodetic mean PM curves around the sharp bend. The large black squares on each of the curves mark the subinterval boundary closest to 1996.0. Table 3 lists the epochs of these subinterval boundaries for each solution in column 3. With this information we conclude that the change of direction in mean PM took place around 1995–96. The figure also shows

[7] therefore, the CSR solution was included.

Table 3
Series start, subinterval boundary closest to 1996.0 for ERP series in Fig. 5 (bottom).

ERP series	Start	Subinterval boundary closest to 1996.0
IVS	1984.0	1996.0
USNO	1979.6	1995.7
CSR	1976.4	1996.1
C04	1962.0	1995.5
IDS	1993.0	1995.5
CODE	1993.6	1996.2

the consistency of mean PM motion derived from the space-geodetic solutions: all positions referring to the epochs in Table 3 lie within a circle of about 1 mas radius. In view of the epoch differences between different dots on the curves referring to one and the same solution in Fig. 5 (bottom) one also concludes that mean PM was rather slow between 1994 and 1997. The DORIS-derived mean PM curve (cyan), based on the input series ids18wd01 (Table 2), is interesting, because it starts on January 3, 1993, thus roughly 0.6 years (corresponding to about 7.5 months) earlier than the CODE-derived mean PM curve and shows no abrupt changes of direction. The CODE-derived mean PM also shows a bend, which points, however, into the opposite direction compared to the other solutions (except DORIS). The DORIS and CODE peculiarities ask for an explanation.

Fig. 6 compares mean PM as derived from the three versions of the DORIS PM series provided in Table 2 and labelled IDS18, IDS19, and IDS19-s with a special version of the CODE series, labelled COD-19 in Fig. 6. The latter solution is based on the CODE PM input data in the interval (1993.6–2019.6). COD-19 thus has the same endpoint of the input data as the DORIS solutions IDS19, IDS19-s. The IDS18 solution thus is the same as the DORIS cyan curve in Fig. 5, which has the endpoint 2018.0. The blue and magenta solutions IDS19 and IDS19-s illustrate mean PM derived from the DORIS solution IDS19, where the time interval of the input data used for their generation are (1993.0–2019.5) and (1993.0–2019.5), respectively. The COD-19 and the IDS19 mean PM curves were used in Fig. 6 to exclude differences caused by the data input interval (Fig. 4 showed, after all, that this aspect matters).

Fig. 6 reveal the following facts: (a) the mean PM curves based on IDS18 and IDS19 (cyan and the blue curves), are almost the same initially, let us say between 1993.0 and 2000.0. (b) The mean PM curves based on IDS19, IDS19-s (blue and magenta), and on COD19 (red), almost coincide towards the end of mean PM curves and hardly can be distinguished in Fig. 6. (c) Mean PM based on COD-19 and on IDS19-s, which are based on the same starting epoch are very close to each other between 1993.6 and, let us say, 2000.0. The starting points of the input PM curve thus have a significant impact on the mean PM curve between 1993 and about 1998. This peculiarity

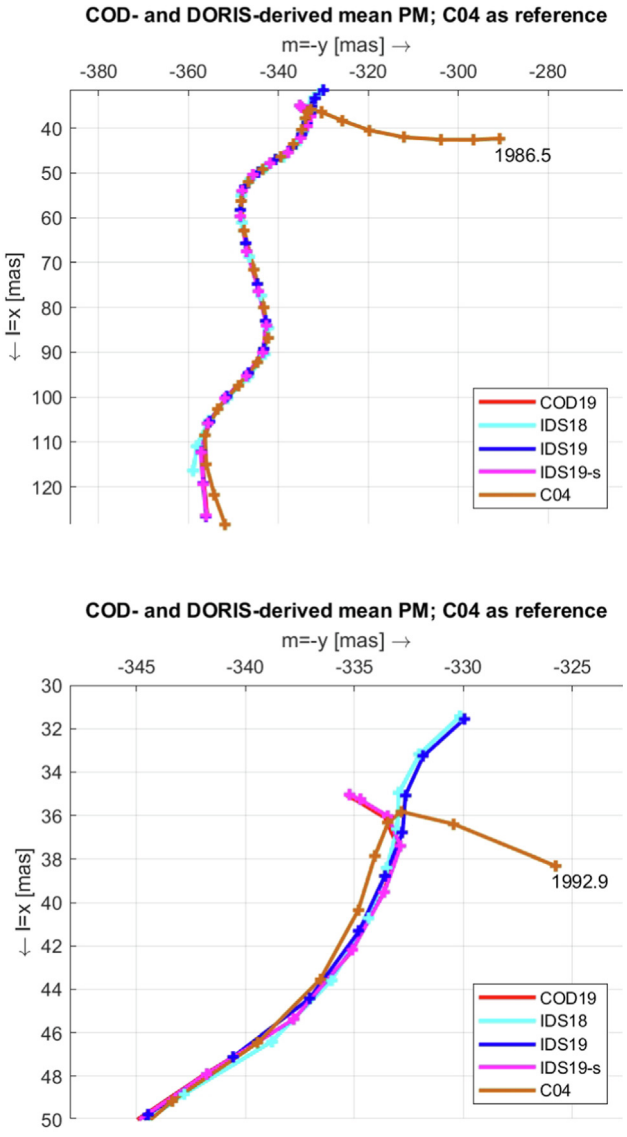

Fig. 6. Mean PM in mas resulting from CODE (1993.6–2019.5) (COD19, red) and three versions of DORIS PM series (ids18wd01, cyan), (ids19wd01, blue), (ids19wd01-s, magenta); IERS 14 C04 series included for reference; top: full series; bottom: zoom around sharp bend. (For interpretation of the references to color in this figure legend, the reader is referred to the web version of this article.)

can be explained: the starting points of the CODE and DORIS PM series in Fig. 6 are very close to the sharp bend of the mean PM curve (shown by the C04-curve), where the "true" direction of mean PM is poorly determined.

Fig. 6 thus explains the behavior of the DORIS and CODE mean PM curves in Fig. 5, which has nothing to do with the underlying space techniques, but merely is a consequence of the fact that the actual mean PM has a sharp bend near the initial epoch of the CODE and DORIS PM series.

Let us now study the velocity of mean PM in more detail. Fig. 7 shows the annual velocities v_l, v_m in the components, and $v_a = \sqrt{v_l^2 + v_m^2}$ of mean PM along the arc in units of mas/y within the subintervals for the CODE solu-

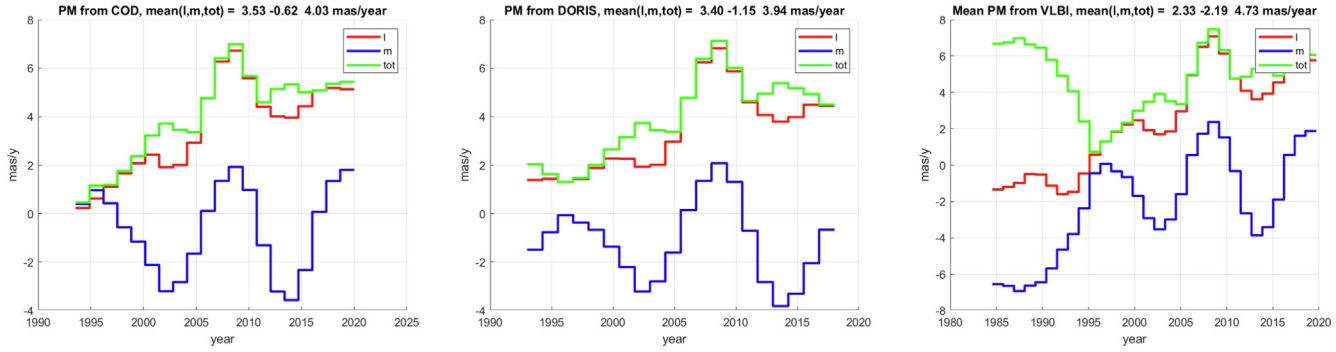

Fig. 7. Left: velocities of mean annual PM 1993.6–2020.0 from CODE PM series; center: velocities of mean annual PM 1993.0–2018.0 from DORIS PM series; right: velocities of mean annual PM 1984–present from IVS PM series.

tion (left), the DORIS solution (center) and the IVS solution (right). The mean values of v_a over all subintervals are measured along the arc – and therefore do *not* correspond to the mean values of v_l and v_m over all subintervals. The velocities are constant within the subintervals in our piecewise linear model, which explains the step functions. The mean values over all subintervals are $\bar{v}_l \approx 3.53\,\mathrm{mas/y}, \bar{v}_m \approx -0.62\,\mathrm{mas/y}$, and $\bar{v}_a \approx 4.03\,\mathrm{mas/y}$ for the CODE solution, $\bar{v}_l \approx 3.40\,\mathrm{mas/y}, \bar{v}_m \approx -1.15\,\mathrm{mas/y}$, and $\bar{v}_a \approx 3.94\,\mathrm{mas/y}$ for the DORIS solution. From these values the meridian of mean PM may be calculated as $\arctan(\bar{v}_y/\bar{v}_x) \approx 10.0°$ West for the CODE-derived mean PM, and 18.7° West for the DORIS solution. The differences are due to the fact that the DORIS ERP series ends around the beginning of the year 2018 as opposed to the CODE series, which ends at the end of 2019.

Fig. 7 (right) providing the velocities for the IVS solution shows a good agreement with the DORIS and the CODE solutions after 1995, but it also shows that the velocities have quite a different pattern prior to 1995, as already expected from Fig. 5: whereas all solutions in Fig. 7 show more or less a constant increase of the velocity v_a along the mean PM trajectory, the IVS solution show a steep, accelerating decrease of the total velocities between 1989 and 1995. All in all, Fig. 7 seem to indicate that a linear model of mean PM motion is questionable. Note, however, that a more linear model can be enforced by increasing the factor f.

Let us conclude the discussions concerning the sharp bend around 1995–96 with the observation that quite a few analysts & organizations reported an unexpected behavior of mean PM early in the 21st century:

- The IERS replaced its linear model in time (McCarthy et al., 2003, Section 7, Eqs. (23,ab)) for the mean pole coordinates by a polynomial of degree 3 (Petit and Luzum, 2010) in the transition from the IERS Conventions 2003 to the IERS Conventions 2010. Note, however, that the IERS abandoned the concept of mean PM in favor of secular PM, which is constant over very long times. Instead of mean PM the term *filtered PM* is now used.
- Chen et al. (2013, Fig. 2) state that the mean pole moved along the meridian at 70° West prior to 2005, approximately along the meridian at 15° East afterwards. Our model very roughly shows a similar mean PM, but only between 2005 and 2010, to switch back to a more Westerly motion afterward (Fig. 3). According to our model there are several sharp bends between 1994 and 2000, where excursions to the East are followed by excursions to the West. Our model, based on ten more years of PM monitoring, thus cannot confirm the results by Chen et al. (2013, Fig. 2), in particular not their interpretation as a secular changes of mean PM.
- Seitz and Müller (2016) state that "...over many decades the mean rotation pole moved along the meridian at 76–78° West with a rate of about 3.3 mas/y. Since about 2005 an abrupt change of direction towards the East is observed, which is attributed to the melting of the ice masses over the poles, leading to a change of sea-level ..." (translated from German). Our model does not confirm such a secular change of mean PM around 2005 either.
- Wahr et al. (2015) analyzed (inter alia) the PM series (IERS C04) of the IERS from 1976–2014, filtered the series using a 435 day half window and concluded that "Starting around 2000, though, there was a significant change in the IERS slopes (of mean pole positions) for both $l(t)$ and $m(t)$ (called m1 and m2 by Wahr et al. (2015)). This change was presumably caused by variations in the distribution of mass at the Earth's surface". Our model roughly confirms the behavior of IERS 14 C04 PM, but assigns the change of the slope not to the year 2000, but to 1995–96.

All analysts cited above had no doubt that an apparent change of mean PM near the beginning of the 21th century is real and has geophysical causes. Our analyses based on many PM series covering the time interval 1962–2020 show

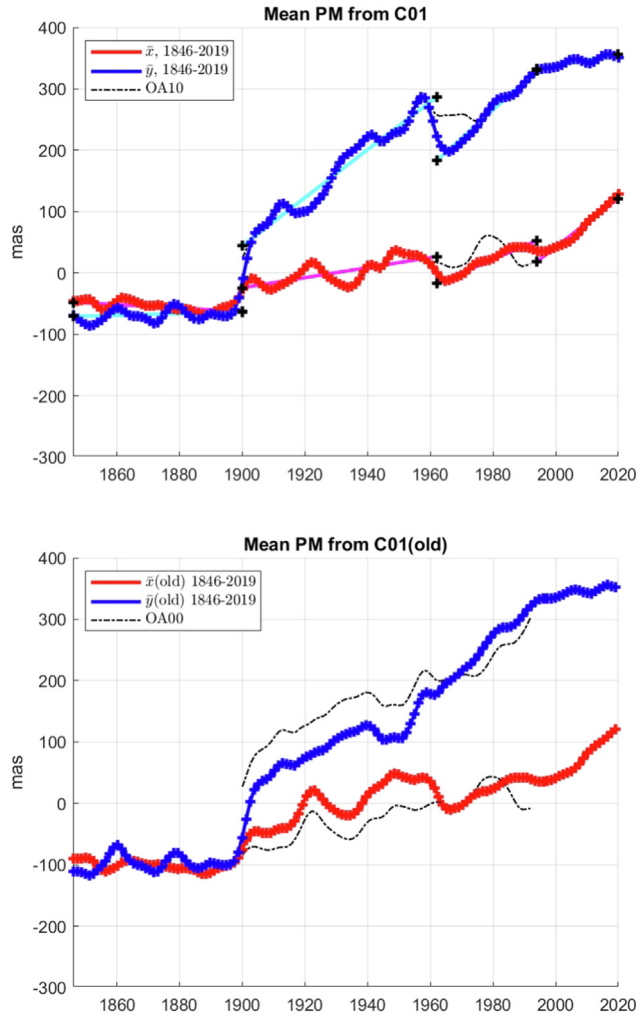

Fig. 8. Mean PM from C01, 1846–2020.0. Top: C01 version after December 2018 (red, blue), and separately in the intervals 1846–1900, 1900–1962, 1962–1994, 1994–2019 (magenta, cyan); black, dash-dot: astrometric PM, based on series OA10; bottom: C01 version prior to December 2018 (red, blue), black, dash-dot: astrometric PM, based on series OA00. (For interpretation of the references to color in this figure legend, the reader is referred to the web version of this article.)

a sharp bend around 1995/96. This bend may or may not be related to the apparent changes of mean PM in the above list. From the point of view of metrology we believe that the geophysical interpretation for the apparent secular change of mean PM is premature – one should be alarmed by the circumstance that the sharp bend around 1995–96 coincides with the advent of the GPS technique used for PM monitoring, which undoubtedly had a heavy impact also on the combined IERS solutions and the definition of the ITRF. We believe that detailed studies, in particular of the methods used for and the results of the VLBI and SLR solutions, are necessary.

Mean PM based on C01 and pure astrometry solutions. Let us now study mean PM resulting from the IERS C01 IAU2000 series (Table 1, series No. 3). Fig. 8 (top) shows the estimated mean PM curves, red for the $\bar{x}$, blue for the $\bar{y}$ components, calculated from the IERS C01 IAU2000 PM series, as it is published by the IERS since the end of December 2018. Fig. 8 (bottom) provides the same information using the same color code for the C01 series as made available by the IERS prior to this date. Mean PM emerging from the C01 series is modeled in the same way as mean PM emerging from the space-geodetic series in Fig. 5, i.e., as a piecewise linear function with a subinterval length $\Delta t \approx 1.3$ years and the filter based on Eqs. (6), (10) with $f = 10$.

The two C01 versions differ substantially in both, offset and rate, in the time interval 1900–1961. The astrometry-derived mean PM shown in Fig. 8 (top) as black dash-dot line was derived from the solution OA10, in Fig. 8 (bottom) from OA00. The two astrometry-derived ERP series were analyzed in the same way as the C01 series. Mean PM, as extracted from the OA10 and the new IERS C01 series perfectly match between 1900 and about 1960. As expected, the two mean PM estimates differ afterwards. The $\bar{y}$ components estimated from the C01 and the OA10 series again agree very well in the interval 1978–1992, after a transition period between 1960 and 1978. This good agreement is probably owed to the procedure to refer the OA10 solution to the ITRF using the time interval between 1978 and 1992, the end of the OA series. One would expect that OA00 and the old version of the IERS C01 ERP series also perfectly match between 1900 and 1960. Fig. 8 (bottom) shows, however, that this is not the case. The differences might be removed to a large extent by removing an offset. It is remarkable, however, that the OA00- and C01-derived mean x-positions match perfectly between 1962 and about 1978, which indicates where the C01 curve stems from in this time interval.

Fig. 8 (top, bottom) also show that the two C01 versions are not identical in the 19th century. Both mean PM values are at the level of about -50 mas in the new C01 version, at a level of about -100 mas in the old version. Also, the excursions from the mean values are larger in the new C01 version.

Two features stand out in Fig. 8 (top): (1) prior to 1900 the rates of mean PM are "practically" zero; (2) the $\bar{y}$-coordinates of PM between 1900 and 1962 show an offset of about 100 mas w.r.t. the mean PM positions in the adjacent time periods. The question must be asked whether the two features are artifacts or real. Property (1) must be an artifact, the alternative simply is not credible. It must be attributed to the analysis applied for this time period by Rykhlova (1969).

Let us now focus on feature (2): Fig. 8 (top) also shows the estimates of mean PM as linear functions of time, in magenta and cyan for $\bar{x}$ and $\bar{y}$, respectively, separately and independently for the time periods 1846–1899, 1900–1961, 1962–1993, 1994–2020.0. The analysis is an application of Eqs. (4), (5) with $n_s = 1$ for mean PM; the conventional 1.3-year spacing was used for the other defining parameters. The endpoints of the estimates are marked with black crosses "+".

Table 4
Mean PM offset differences at boundaries.

Boundary	Parts	$\Delta\bar{x}$ (mas)	$\Delta\bar{y}$ (mas)
1900.0	2-1	38	108
1962.0	2-3	44	104
1994.0	3-4	34	2

Table 5
Mean PM rates in intervals, corresponding meridian.

Interval	$\dot{\bar{x}}$ (mas/y)	$\dot{\bar{y}}$ (mas/y)	Meridian deg W
1846–1899	−0.3	0.2	–
1900–1961	0.7	3.9	79.8
1962–1993	2.2	4.6	64.4
1994–2019	4.0	0.9	12.7

The subdivision of the C01 series into four parts is motivated by the IERS document EOPC01.guide[8] describing the key features of the C01 PM series. This document says that the C01 series is composed of three substantially different parts, namely the time periods 1846–1899, 1900–1961, 1962–today. Between 1962 and 2020, the C01 series actually consists of a down-sampled version of the IERS 14 C04 series. Within this third interval, the starting point of the GNSS contributions is mentioned as well as an essential epoch & event.

Ideally, the endpoints of the linear estimates from two adjacent intervals should coincide. Fig. 8 (top) shows that this is definitely not the case. The mismatch is substantial at the left and right boundaries of the interval 1900–1962, in particular for the $\bar{y}$ component. By a parallel displacement of about −100 mas, the $\bar{y}$ component fits much better to the linear fits of the two adjacent intervals. This result seems to indicate that property (2) of the mean PM curve might be an artifact as well.

Table 4 lists the offsets at the three inner boundaries of the four parts of C01, Table 5 provides the mean rates within the four parts. Both characteristics stem from the analysis in the four time periods. Fig. 8 (top) and Tables 4, 5 are the motivation to create a modified C01 series by shifting all PM positions of the analyzed C01 series between 1900.0 and 1962.0 by −41 mas in the $\bar{x}$-direction and by −106 mas in the $\bar{y}$-direction. Also, the mean rates of 0.7 mas/y in x and 3.9 mas/y in y, as established by C01 series in the period 1900–1962, are added to the observations in the 19th century.

The mean rates and meridians in the last two intervals in Table 5 may be compared to the rates obtained by Roy and Pelletier (2011) in the two time intervals 1976–1992 and 1992–2009. These values are $(\dot{\bar{x}}, \dot{\bar{y}})$=(1.7, 4.1) mas/y in the first interval, $(\dot{\bar{x}}, \dot{\bar{y}})$=(0.9, 1.5) mas/y, resulting in the meridians 68° West and 58° West before and after 1992. Whereas the agreement is quite good in the first interval, the agreement is rather poor in the interval from 1992 onwards. The application of our model to the pole series SPACE2008 might give more insight.

Fig. 9 (top) shows the $\bar{x}$ and $\bar{y}$ values from the C01 solution modified in this sense, from 1846 to 2019, as the red curve. The analysis features were the same as those underlying Fig. 8. The mean PM positions emerging from our analysis of the OA10 solution are included as well, as

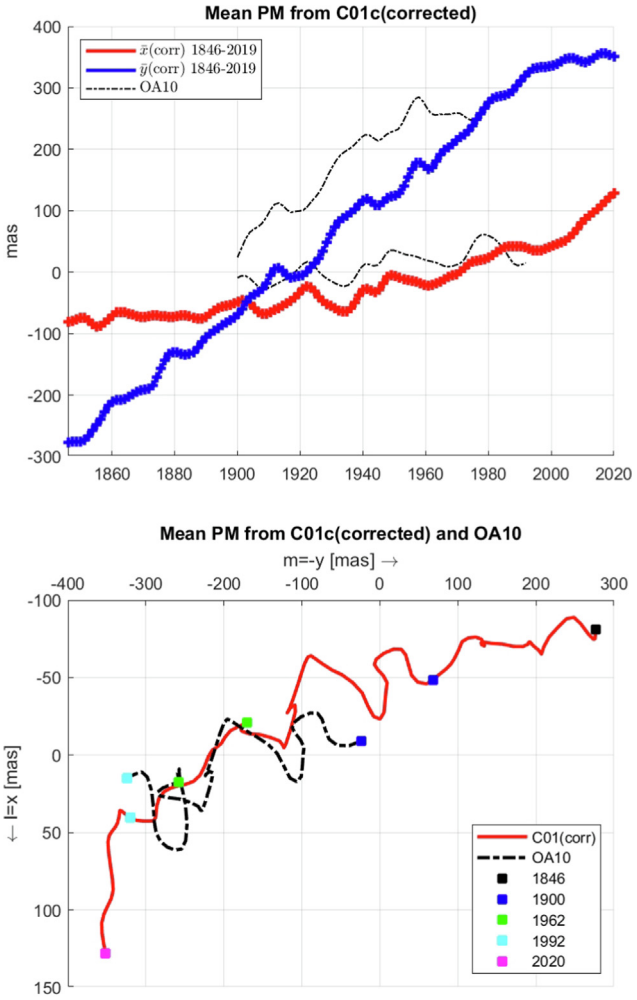

Fig. 9. Top: Mean PM 1846–2019.8 from C01, version after December 2018 (red, blue), offset in interval 1900.0–1962.0 removed using Table 4, rate in 19th century applied using the rates in 1900–1962, Table 5; black, dash-dot: astrometric mean PM 1900.0–1992.0, based on series OA10; bottom: same mean PM 1846–2019.8 from C01 as a map. The colored squares in the bottom figure mark few selected epochs. (For interpretation of the references to color in this figure legend, the reader is referred to the web version of this article.)

dash-dot lines. Fig. 9 (bottom) shows the paths of mean PM of the modified C01 (red) and of the OA10 ERP series (black, dash-dot). Between 1900 and 1960 the corrected C01 curve is in good approximation a parallel shifted version of the OA10 solution – as it should be according to the above considerations. After 1960 the shapes of the two curves differ substantially. The total lengths of the two

[8] https://hpiers.obspm.fr/iers/eop/eopc01/EOPC01.guide.

mean PM trajectories between 1900 and 1962, measured as straight lines between the blue and green dots on the two trajectories, is about the same, whereas the lengths between 1962 and 1992 differ substantially – the OA10-derived distance (on the black curve) is much shorter than the C01-derived distance. Time tags at selected epochs are provided as colored squares on the two mean PM curves of Fig. 9 (bottom).

Figs. 8 (top, bottom) and Fig. 9 show the time evolution of three different versions of the C01 mean PM components. As the scale and the span of values on the vertical axes is the same in the three cases, one can easily compare the coordinate values for any epoch. This is in particular true for the epoch 1900.0, where the PM curves should cross the CIO-pole with the coordinates $(\bar{x}, \bar{y}) = (0, 0)$. Obviously, this is not the case for any of the three C01-versions. As we have no responsibility for the C01-versions in Fig. 8 and as the version underlying Fig. 8 was created by applying the empirically determined offsets in Table 4 we cannot explain the offsets by geodynamic argumentation.

The red curve in Fig. 9 (bottom) should be viewed as an *educated guess* of mean PM between 1846.0 and 2020.0 using the current C01 ERP file, with only two modifications (Tables 4 and 5).

5.2. Chandler and annual motion

The defining parameter functions of the annual and Chandler motions in Eqs. (4) are the initial annual component functions $l_{y0}(t), m_{y0}(t)$ and the initial Chandler component functions $l_{C0}(t), m_{C0}(t)$. According to Eqs. (5) these functions are piecewise linear and continuous, their values at the subinterval boundaries are the actual parameters in the estimation process. After parameter estimation one may calculate the classical parameters, namely the amplitudes $\rho_{y0,i}, \rho_{C0,i}$ and the phases $\phi_{y0,i}, \phi_{C0,i}$. Subsequently, both parameter types are analyzed.

The CODE solution 1993.6 to 2020.0 Fig. 10 (top) shows the initial annual (red) and Chandler component functions (blue), when analyzing the CODE PM series (Table 1, series No. 1). The resulting amplitudes are also provided as solid lines. The blue curves are shifted by 1" (1 arcsec), for better visibility. Whereas the variation of the initial components and of the amplitude is rather small for the annual motion, we see a net decrease in absolute value from about 200 mas to about 20 mas, in both initial Chandler components from 1993.6 to 2020.0.

Fig. 10 (bottom) gives a detailed view of the Chandler components and of the corresponding amplitude, as a function of time. Obviously, any attempt to model PM with a constant Chandler amplitude must fail, at least in this time interval.

Figs. 11 show the time development of the traditional parameters, the initial amplitudes (top) and phases (bottom) associated with the initial annual and Chandler motions. The red curves characterize the annual motion,

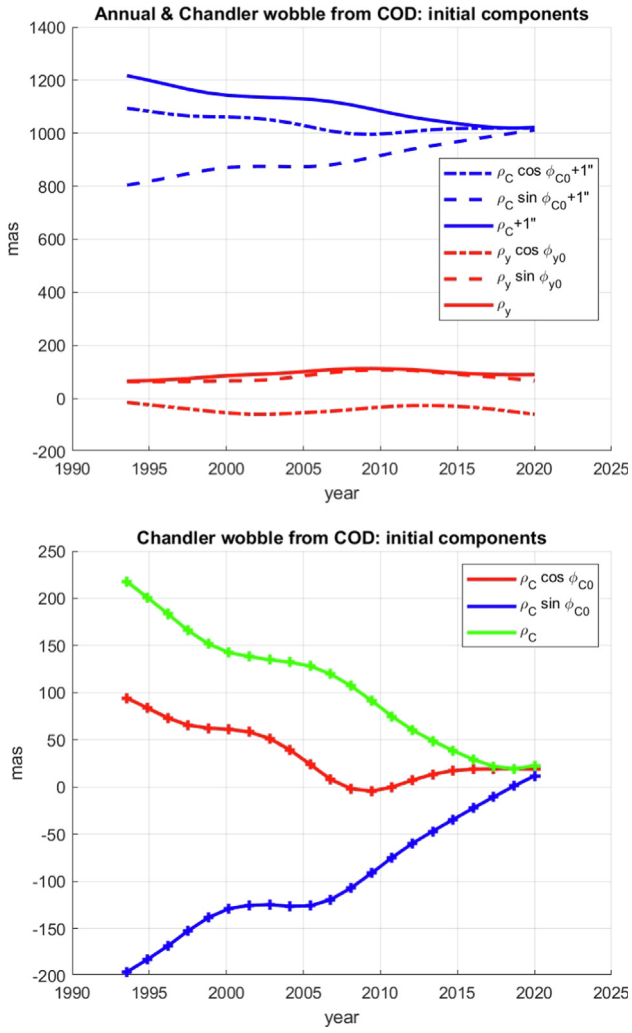

Fig. 10. Analysis of CODE PM series (Table 1, series No. 1). Top: initial annual components (red) and initial Chandler components (blue), and corresponding amplitudes, Chandler values shifted by 1000 mas; bottom: initial Chandler components and corresponding amplitudes; subinterval boundaries marked by "+". (For interpretation of the references to color in this figure legend, the reader is referred to the web version of this article.)

the blue curves the Chandler motion. Fig. 11 (top) provides the amplitudes, Fig. 11 (bottom) the initial phases as a function of time. The latter figure documents in particular a phase change of about 120° of the Chandler motion between 2010 and 2019. At first sight the massive phase change looks impressive. On the other hand, large phases changes associated with small components are not really impressive on the Earth's surface: Fig. 10 (top) shows that the amplitudes, therefore also the components, do not show any "strange" behavior. Therefore we prefer the defining parameters to characterize the periodic parts of PM. The formal errors $m_{\ldots}$, actually of the values $3m_y$ and $3m_C$ are provided as well in Fig. 11.

Period changes from phase changes. If the phase estimates associated with either the annual or the Chandler ini-

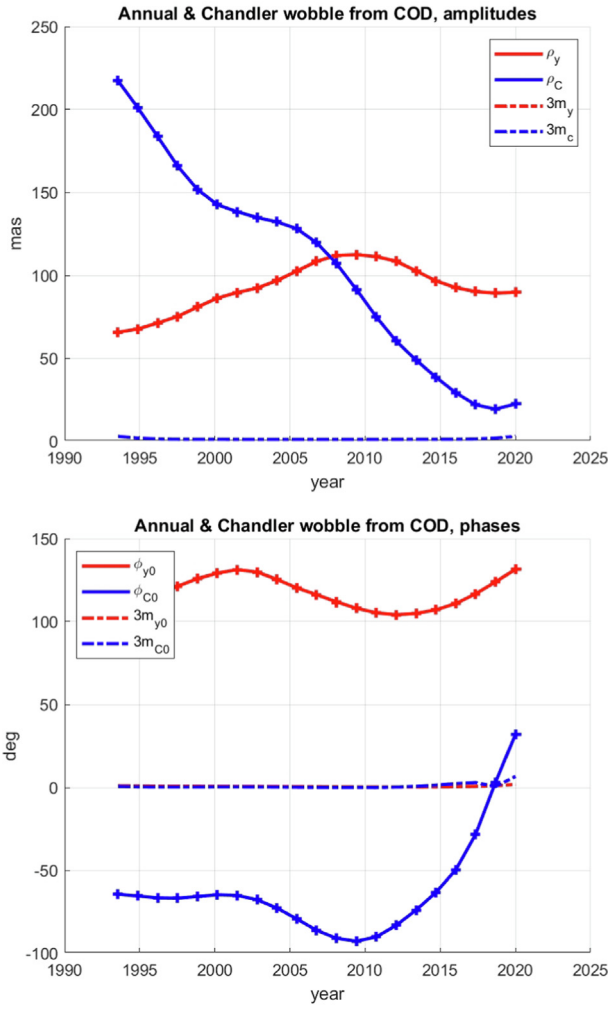

Fig. 11. Analysis of CODE PM series (Table 1, series No. 1). Top: Amplitudes of annual (blue) and Chandler motion (red); bottom: initial phases from initial annual (blue) and Chandler components; subinterval boundaries marked by "+". (For interpretation of the references to color in this figure legend, the reader is referred to the web version of this article.)

tial components do not change between the subinterval boundaries t_{i-1} and t_i, the motion took place with the nominal angular velocity ω in the interval $I_i = [t_{i-1}, t_i]$. If these phases at t_{i-1} and t_i are not the same, however, the mean angular velocity must have been different in the interval, and consequently the mean period of the periodic motion differed from the nominal value as well. From the phase difference $\Delta\phi \doteq \phi(t_i) - \phi(t_{i-1})$ and from the time difference $\Delta t = t_{i-1} - t_i$, one may calculate the change $\Delta\omega$ w.r.t. the nominal mean angular velocity ω in the interval I_i:

$$\Delta\omega = \frac{\Delta\phi}{\Delta t}, \tag{12}$$

where ω may be either the annual or the Chandler angular velocity and $\Delta\phi$ the corresponding phase difference between the epochs t_i and t_{i-1}. The corresponding change in the period is obtained by taking the total differential of the relation $P = 2\pi/\omega$:

$$\Delta P = -\frac{2\pi}{\omega^2}\Delta\omega = -P\frac{\Delta\omega}{\omega}. \tag{13}$$

Fig. 12 shows the changes of the annual (red) and the Chandler (blue) periods w.r.t. the nominal periods in the subintervals obtained by applying formula (13) to the difference of the angular velocities calculated with Eq. (12). Fig. 12 (top) shows the period changes when analyzing the CODE solution (1993.6–2020.0), Fig. 12 (bottom) when analyzing the solution OA10 (1900.0–1992.0). Both figures document relatively small changes of the annual periods and one major change of the Chandler period in each of the time intervals, in about 2018 for the CODE GNSS analysis, in about 1927 for the analysis based on optical astrometry. The maximum change of the Chandler period for the 2018 event is about −35 days, implying that the actual Chandler period within this interval is about 398 days. The maximum change for the 1927 event is even somewhat larger, about −41 days, implying that the Chandler period was about 382 days in 1927. The Chandler period was/is thus getting rather close to the annual period in both cases, implying that it becomes difficult to separate

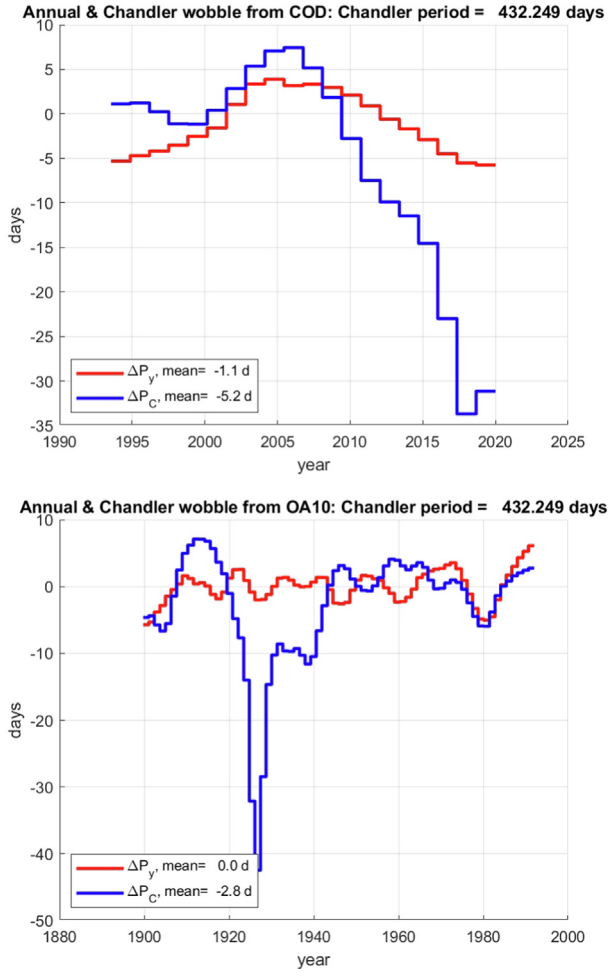

Fig. 12. Change of annual and Chandler periods from phase changes; top: from CODE solution 1993.6–2020.0, bottom: from solution OA10, 1900–1992.

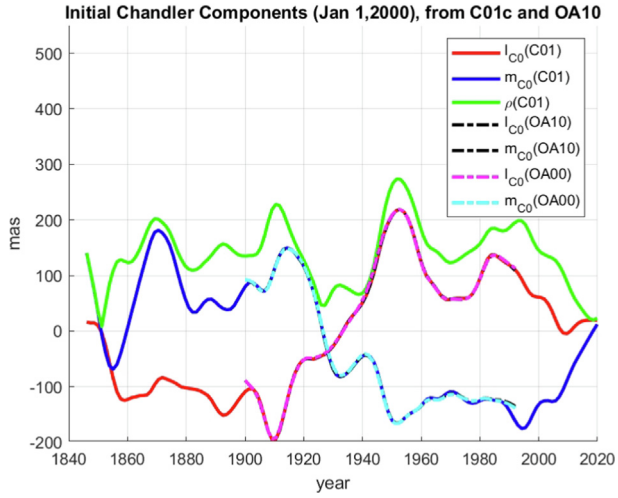

Fig. 13. Initial Chandler component functions from C01, OA00, and OA10.

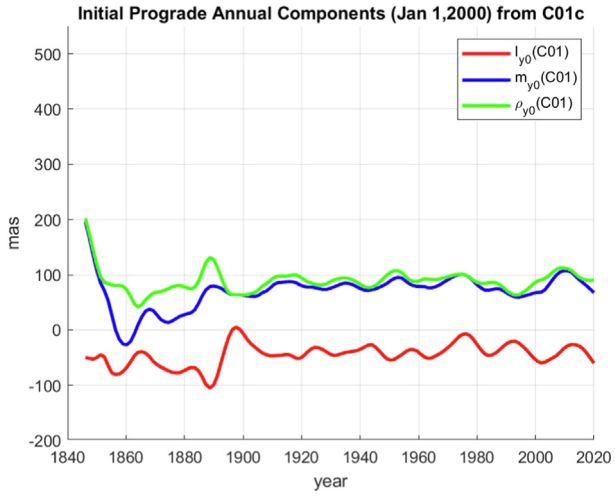

Fig. 14. Initial annual component functions from C01.

the two motions in the analysis. The pattern of the annual periods in Fig. 12 (top), following to a minor extent the pattern of the Chandler period, might be a consequence of this problem. The Chandler amplitudes, thus also the components, are close to zero near both epochs. The two events are separated by about 92 years. Knowing that two pronounced minima of the Chandler amplitudes occurred around 1927 and 2018, Figs. 12 also tell that there is a clear correlation between the Chandler amplitudes and the Chandler periods. Deep minima occur while the amplitude is small. Note that this result is opposed to the result postulated by Guinot (1972).

The C01 series 1846–2019 and the solutions OA00, OA10 1900.0–1992.0 (Table 1, series Nos. 3, 4, 5). Fig. 13 shows the initial Chandler component functions $l_{C0}(t), m_{C0}(t)$ for the solution IERS C01 IAU2000. They were generated with the modified C01 ERP series. The same figure also shows the Chandler component functions emerging from the two astrometric series OA0 and OA1. As opposed to mean PM in Fig. 9, where substantial differences between the series based on astrometry and the C01 series were observed, the agreement between the three series is usually below the 1 mas level in the entire common interval 1900.0–1992.0. The agreement is in particular remarkable in the time interval 1976.0–1992.0, where the C01 series are believed to be independent of astrometry. Fig. 13 therefore documents the value of optical astrometry for PM monitoring.

The main message of Fig. 13, however, are the variations with a period of about 170–190 years in the initial Chandler components. It is not trivial to extract a precise period from Fig. 13, because this period is of the order of the total length of the entire C01 PM series (about 174 years). Also, the first years of the C01 series, let us say, between 1846 and 1861, i.e., prior to the data gap between November 1858 and November 1860, are not really of the same quality as the remaining part of the series. The best estimate for the longest period of the initial Chandler components from Fig. 13 is probably twice the time period between the 1926 and the 2018 epochs with small Chandler components and amplitudes, i.e., about $\tilde{P} \approx 2 \cdot 92 = 184$ years.

Fig. 13 also shows $\rho_{C0}(t) = \sqrt{l^2_{C0}(t) + m^2_{C0}(t)}$, i.e., the amplitude associated with the initial Chandler components, as the green curve. As the components have to be squared to get the amplitudes, the main period of the amplitudes is half the period of the components, i.e., about 85–95 years.

Fig. 14 shows that the initial annual component functions from C01 do not show similar long-term periodic variation as the initial Chandler functions in Fig. 13. The variations with a period of about 20 years and unexplained variations in the 19th century deserve further investigation.

The composite nature of the Chandler motion. The largest time variations of $l_{C0}(t), m_{C0}(t)$ in Fig. 13 resemble the pattern obtained by a superposition of two Chandler signals with slightly different periods P_{C_1}, P_{C_2}. The two periods cannot be extracted directly from Fig. 13. What we see in this figure is their beat period, the mentioned period of about 170–190 years.

A better estimate of this period $\tilde{P}$ is obtained by analyzing directly the spectrum of the PM components $l(t) - \bar{l}(t)$ and $m(t) - \bar{m}(t)$ (mean PM according to Eq. (4)) of the C01 solution. Mean PM according to the piecewise linear model was thus subtracted from the original PM series. We now spectrally analyze the input PM series reduced by mean PM, implying that – in this paragraph only – the principle stated in Section 1 to deal only with the long-term aspects of PM is abandoned.

In order to generate a correct spectrum, the missing data in the gap between November 1958 and November 1960 were padded as zero values. Moreover, the C01 series from 1900 onwards was down-sampled by a factor of 2 to get an ERP series with an equidistant spacing from 1846 to 2019.

Fig. 15 (top) shows the spectra of the components (red and blue) and of the amplitude (green) in the range

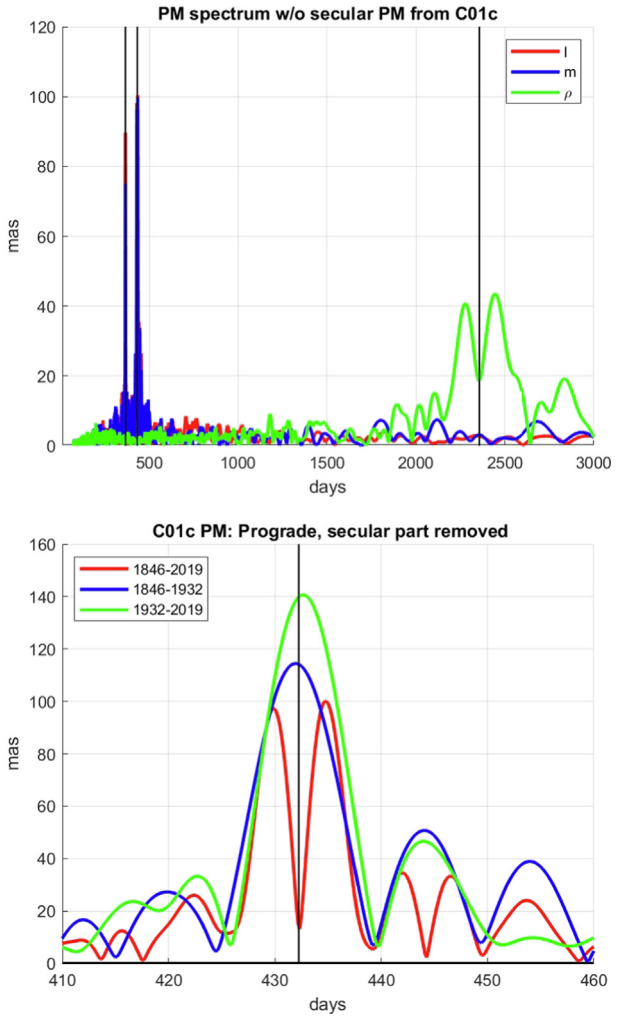

Fig. 15. Amplitude spectra of the PM coordinates emerging from the C01 series; top: PM components l, m, and associated amplitudes; bottom: prograde components of PM referring to three time intervals.

between 0 and 3000 days (8.2 years) resulting from an analysis of the full time period 1846–2019. The three black vertical lines mark the periods of the nominal annual and Chandler motions, and the resulting beat period of $P_b = \frac{P_y P_C}{P_C - P_y} = 6.45$ years of the annual and conventional Chandler motion. The spectrum of the amplitudes (green) does not show one, but two spectral lines around the expected period P_b, which are separated by $\Delta T_b \approx 169$ days, indicating the existence of a split Chandler motion as postulated by Chandler (1901). From the two beat periods associated with the two Chandler periods P_{C_1}, P_{C_2}

$$P_{b_i} = \frac{P_y P_{C_i}}{P_{C_i} - P_y}, i = 1, 2,$$

we obtain

$$P_{C_i} = \frac{P_{b_i} P_y}{P_{b_i} - P_y}, i = 1, 2,$$

and eventually

$$\Delta P_C \doteq P_{C_2} - P_{C_1} = \frac{P_y^2 (P_{b_1} - P_{b_2})}{(P_{b_1} - P_y)(P_{b_2} - P_y)} \approx 5.7d. \quad (14)$$

Formula (14) assumes that both beat periods $P_{b_i}, i = 1, 2$, and not only their difference are known. Neglecting higher order terms, these can be approximated with sufficient accuracy by $P_{b_i} = P_b \pm \frac{\Delta T_b}{2}$.

Fig. 15 (bottom) shows a detailed view of the amplitude spectrum of PM around the period P_C. The spectrum refers to prograde PM in the (l, m)-plane. Only when analyzing the entire time interval 1846–2019, a "bifurcation" of the Chandler spectrum, as described by Fedorov and Yatskiv (1965) and other authors, becomes apparent. When either analyzing the first or the second half of the ERP series, only one spectral line close to the nominal period with an enlarged amplitude, compared to the amplitudes of the two split signals (red), remains. This behavior explains some of the difficulties to decide whether or not the bifurcation of Chandler motion is real (Fedorov and Yatskiv, 1965). In any case we may directly extract the separation of the two Chandler signals from Fig. 15 (bottom) as $\Delta P_C{\prime} \approx 5.0$ days. This is about 12% below the value emerging from Eq. (14). Subsequently, we use the value emerging from Eq. (14) because it is much less dependent on the length of the PM series. The beat period of the two Chandler periods is:

$$\begin{aligned} P_{b;C1,C2} &= \frac{P_{C1} P_{C2}}{P_{C2} - P_{C1}} \\ &= \frac{(432.25 - 2.85)(432.25 + 2.85)}{5.7} \\ &\approx 32778 \text{ days} \doteq 90 \text{ years} \end{aligned} \quad . \quad (15)$$

We have analyzed the fine structure of the spectral line resulting from the analysis of the C01 PM series. The structure of the spectral line around the Chandler period is in essence that of a PM series consisting of a Chandler motion consisting of two waves separated by 5–6 days. Fig. 24 of Section 6.3 will show that a simulated PM series consisting of two Chandler-like signals separated by 5.7 days in period results in a spectral line with the same fine structure as in Fig. 15 (bottom).

Let us designate the angular velocity corresponding to the period $P_{b;C_1,C_2}$ as

$$\Delta\omega \doteq 2\pi / P_{b;C1,C2}. \quad (16)$$

The term "bifurcation" implies that the Chandler motion has a fine structure. Chandler (1901) was probably first to advocate such a behavior. In the cited paper he wrote "in addition to the 428-day and the annual components of the polar motion, already made known, there is a third component with a period of 436 days, and an amplitude of 0".09,[9] thus considerably smaller than that of the other terms. The evidence is very extensive, and extremely clear, …" (Chandler, 1901). According to Chandler the separation of the two Chandler periods is thus 8 days –

[9] Chandler assumed a value 0".140 for his 428 day term.

pretty close to our value (14) of 5.7 days. Let us give additional evidence supporting a fine structure of Chandler motion.

Alternative model for Chandler motion. Eqs. (17) represent an alternative version for the Chandler part of the PM model (4), (5). The alternative model is based on a two-dimensional Fourier series implying periodic extension beyond the range of the observed PM series. The alternative model represents the Chandler part of PM motion by real analytic functions, allowing a comprehensive analysis of its periodicity. The model is purely empirical in nature and it is not based on geophysical considerations.

For $n = 0$, the new model (17) is the same as the Chandler part in Eq. (3), for $n = 1$, without the term with $k = 0$, the model is that proposed by Chandler (1901), representing the Chandler motion by two constituents, namely for $k = \pm 1$, separated in our case by 5.7 days, and not by 8 days as proposed by Chandler. All other cases are generalizations w.r.t. these two simple cases.

$$\begin{aligned} l_C(t) &= \sum_{k=-n}^{n} \tilde{\rho}_{Ck} \cos\left[\left(\omega_C t + \tfrac{k}{2}\Delta\omega t\right) + \tilde{\phi}_{Ck}\right] \\ m_C(t) &= \sum_{k=-n}^{n} \tilde{\rho}_{Ck} \sin\left[\left(\omega_C t + \tfrac{k}{2}\Delta\omega t\right) + \tilde{\phi}_{Ck}\right] \end{aligned} \quad . \tag{17}$$

The symbols $\tilde{\rho}_{\ldots}$ and $\tilde{\phi}_{\ldots}$ are used to distinguish the amplitudes and phases related to the alternative model from the amplitudes and phases of the standard model (1). Eqs. (17) may be used for parameter estimation after replacing the amplitudes $\tilde{\rho}_{Ck}$ and the initial phases $\tilde{\phi}_{Ck}$ by the initial components $\tilde{l}_{Ck} = \tilde{\rho}_{Ck}\cos\tilde{\phi}_{Ck}$ and $\tilde{m}_{Ck} = \tilde{\rho}_{Ck}\sin\tilde{\phi}_{Ck}$ using Eqs. (2):

$$\begin{aligned} l_C(t) &= \sum_{k=-n}^{n} \left[\tilde{l}_{Ck}\cos\left(\omega_C + \tfrac{k}{2}\Delta\omega\right)t - \tilde{m}_{Ck}\sin\left(\omega_C + \tfrac{k}{2}\Delta\omega\right)t\right] \\ m_C(t) &= \sum_{k=-n}^{n} \left[\tilde{m}_{Ck}\cos\left(\omega_C + \tfrac{k}{2}\Delta\omega\right)t + \tilde{l}_{Ck}\sin\left(\omega_C + \tfrac{k}{2}\Delta\omega\right)t\right] \end{aligned} \quad . \tag{18}$$

The resulting relationship between the Chandler components $l_C(t), m_C(t)$ and the initial Chandler components is linear. Eqs. (18) thus may be used to determine the parameters of the alternative model in a linear parameter estimation problem.

As opposed to the standard model (3) it does not make sense in the alternative model (18) to make the coefficients time variable. The time variability is already contained in the different angular velocities of the Chandler constituents. For an expansion up to $n = 12$ we thus have $n_p = 2(2n + 1) = 50$ parameters in the alternative model (17), whereas the number of parameters for the Chandler part was 270 when using the conventional model (4), (5) to represent the IERS C01 IAU2000 PM series. The new model thus promises to be more rigid – when applied to the full C01 series. In the results presented subsequently, the alternative model for the Chandler motion was not implemented "from scratch": the conventional models for mean and annual PM based on Eqs. (4), (5) were subtracted from the original observations, the model (18) was then applied to these differences.

Let us provide better insight into the structure of Eqs. (17) by splitting up the angular argument in Eqs. (17) into the angle $\alpha = \omega_C t$ and the angles $\beta_k = \frac{k}{2}\Delta\omega t + \tilde{\phi}_{Ck}$. By applying the transformation represented by Eqs. (2) we obtain:

$$\begin{aligned} l_C(t) &= \sum_{k=-n}^{n} \tilde{\rho}_{Ck}\left[\cos\left(\tfrac{k}{2}\Delta\omega t + \tilde{\phi}_{Ck}\right)\cos\omega_C t - \right. \\ &\qquad \left. \sin\left(\tfrac{k}{2}\Delta\omega t + \tilde{\phi}_{Ck}\right)\sin\omega_C t\right] \\ m_C(t) &= \sum_{k=-n}^{n} \tilde{\rho}_{Ck}\left[\sin\left(\tfrac{k}{2}\Delta\omega t + \tilde{\phi}_{Ck}\right)\cos\omega_C t + \right. \\ &\qquad \left. \cos\left(\tfrac{k}{2}\Delta\omega t + \tilde{\phi}_{Ck}\right)\sin\omega_C t\right] \end{aligned} \quad . \tag{19}$$

Eqs. (19) separate the rapidly time-variable part, represented by the angle $\omega_C t$, and the slowly varying parts, represented by the sin- and cos-functions of the angles $\frac{k}{2}\Delta\omega t + \tilde{\phi}_{Ck}$.

Eqs. (19) obviously may be written as:

$$\begin{aligned} l_C(t) &= \lambda_C(t)\cos\omega_C t - \mu_C(t)\sin\omega_C t \\ m_C(t) &= \mu_C(t)\cos\omega_C t + \lambda_C(t)\sin\omega_C t \end{aligned} , \tag{20}$$

where

$$\begin{aligned} \lambda_C(t) &= \sum_{k=-n}^{n} \tilde{\rho}_{Ck}\cos\left(\tfrac{k}{2}\Delta\omega t + \tilde{\phi}_{Ck}\right) \\ \mu_C(t) &= \sum_{k=-n}^{n} \tilde{\rho}_{Ck}\sin\left(\tfrac{k}{2}\Delta\omega t + \tilde{\phi}_{Ck}\right) \end{aligned} \quad . \tag{21}$$

Eqs. (20) represent a prograde circular motion with a time-variable radius $\tilde{\rho}_C(t) = \sqrt{\lambda_C^2(t) + \mu_C^2(t)}$ and a time variable phase angle $\arctan\left(\frac{\mu_C}{\lambda_C}\right)$. The motion of $\mu(t)$ and $\lambda(t)$ is in general not circular and may be either pro- or retrograde. Note as well that at reference time one obtains from Eqs. (20) for $t = 0$ the relations $l_{C0} = \lambda_{C0}$ and $m_{C0} = \mu_{C0}$.

For illustration, the alternative model (20), (21) is further developed with only the terms $k = -1$ and $k = +1$. Furthermore, it is assumed that $\tilde{\rho}_{C,-1} = \tilde{\rho}_{C,+1} = \tilde{\rho}_{C*}$ and that $\tilde{\phi}_{C,-1} = \tilde{\phi}_{C,+1} = \tilde{\phi}_{C*}$. The hypothetical Chandler motion is thus composed of two constituents with the same amplitudes and with angular velocities differing by $\Delta\omega$ & centered at ω_C. The assumption $\tilde{\phi}_{C,-1} = \tilde{\phi}_{C,+1} = \tilde{\phi}_{C*}$ implies that the radius of the combined two component Chandler motion assumes its maximum value at the newly defined reference epoch, which is thus *not* the same as the reference epoch used so far. Retaining only the terms $k = -1$ and $k = +1$ in Eq. (21) we obtain:

$$\begin{aligned}\lambda_C(t) &= \tilde{\rho}_{C*}\left[\cos\left(-\tfrac{\Delta\omega t}{2}+\tilde{\phi}_{C*}\right)+\cos\left(\tfrac{\Delta\omega t}{2}+\tilde{\phi}_{C*}\right)\right]\\ \mu_C(t) &= \tilde{\rho}_{C*}\left[\sin\left(-\tfrac{\Delta\omega t}{2}+\tilde{\phi}_{C*}\right)+\sin\left(\tfrac{\Delta\omega t}{2}+\tilde{\phi}_{C*}\right)\right]\end{aligned}, \tag{22}$$

or, using once more the relations (2):

$$\begin{aligned}\lambda_C(t) &= 2\tilde{\rho}_{C*}\cos\tilde{\phi}_{C*}\cos\tfrac{\Delta\omega t}{2} = 2\lambda_{C0}\cos\tfrac{\Delta\omega t}{2}\\ \mu_C(t) &= 2\tilde{\rho}_{C*}\sin\tilde{\phi}_{C*}\cos\tfrac{\Delta\omega t}{2} = 2\mu_{C0}\cos\tfrac{\Delta\omega t}{2}\end{aligned}. \tag{23}$$

The amplitude of the two-component Chandler motion with equal amplitudes may thus be calculated as follows:

$$\begin{aligned}\tilde{\rho}_C(t) &= \tilde{\rho}_{C*}\sqrt{4\left(\cos^2\tilde{\phi}_{C*}+\sin^2\tilde{\phi}_{C*}\right)\cos^2\tfrac{\Delta\omega t}{2}}\\ &= \tilde{\rho}_{C*}\sqrt{4\tfrac{1}{2}(1+\cos\Delta\omega t)}\\ &= \tilde{\rho}_{C*}\sqrt{2(1+\cos\Delta\omega t)},\end{aligned} \tag{24}$$

where the trigonometric identity $\cos 2\alpha = 2\cos^2\alpha - 1$ was used.

$\tilde{\rho}_C(t)$ thus assumes the maximum value $2\tilde{\rho}_{C*}$ at the epochs $t_k = \pm k \cdot P_{b;C1,C2}, k = 0, 1, 2, \ldots$, where $P_{b;C1,C2}$ is the period in Eq. (15). The value zero is assumed half way between these epochs. As opposed to the initial components, which have a period of $2 \cdot P_{b;C1,C2} \approx 180$ years, the time-variable amplitude has a period of $P_{b;C1,C2} \approx 90$ years.

The λ_C- and the μ_C-components thus oscillate between the values $\pm 2|\lambda_{C0}|, \pm 2|\mu_{C0}|$, where $2\lambda_{C0}$ and $2\mu_{C0}$ are the values at reference time, $-2\lambda_{C0}, -2\mu_{C0}$ at reference time $\pm P_{b;C1,C2}$ (Eq. (15)), respectively. The period of the initial Chandler component motion is $2P_{b;C1,C2}$. The radius $\tilde{\rho}_C(t)$ of the combined Chandler motion at time t varies between the value $2\rho_{C*}$ and zero, according to Eq. (24).

When the radii $\tilde{\rho}_{C,-1}$ and $\tilde{\rho}_{C,+1}$ differ slightly, the motion takes place in a highly eccentric ellipse in the (l, m)-plane, where the semi-major axis of the ellipse is $(\tilde{\rho}_{C,-1} + \tilde{\rho}_{C,+1})/2$, the semi-minor axis $|\tilde{\rho}_{C,-1} - \tilde{\rho}_{C,+1}|/2$.

Fig. 16 shows the values of the initial Chandler component functions, estimated from the C01 series, emerging from the standard model (solid lines) and from the alternative model (dash-dot lines). The corresponding amplitudes are provided as well (green lines). Fig. 16 (top) compares the components from the conventional model with those emerging from the alternative model (22), (23) with the terms $k = -1$ and $k = +1$, the model proposed by Chandler (1901) – with (hopefully) improved periods and amplitudes. The figure shows the main periods of 180 years for the components and the period of 90 years for the amplitudes. Fig. 16 (bottom) provides the same information as Fig. 16 (top), but uses the full alternative model (17) up to $n = 12$. Except for the early years, the agreement between the standard and the alternative model is almost perfect in Fig. 16 (bottom).

Fig. 17 shows the amplitudes $\tilde{\rho}_{Ck}$ obtained from the components of the individual terms of the alternative

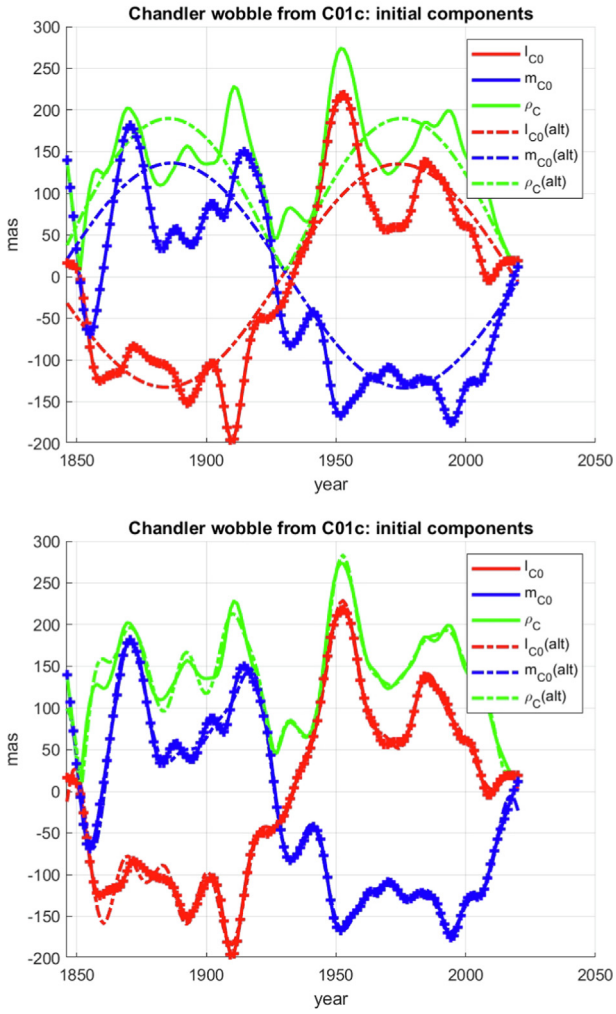

Fig. 16. Components of initial Chandler motion from conventional and alternative model. Top: Chandler's two component Chandler motion, bottom: Alternative model (17) with $n = 12$.

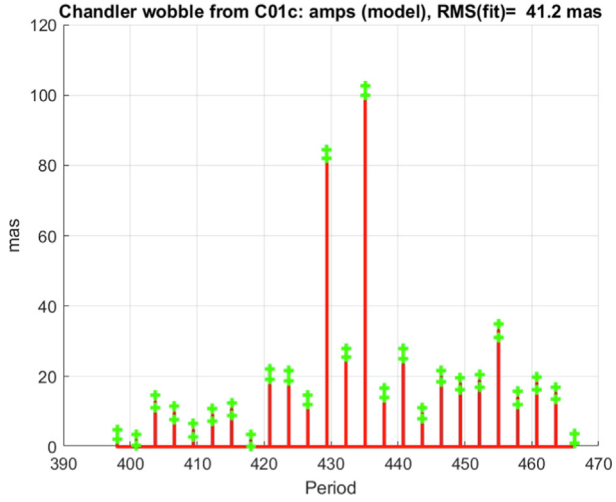

Fig. 17. Estimated amplitudes using the alternative model (17) with $n = 12$, represented as a function of the corresponding periods in days.

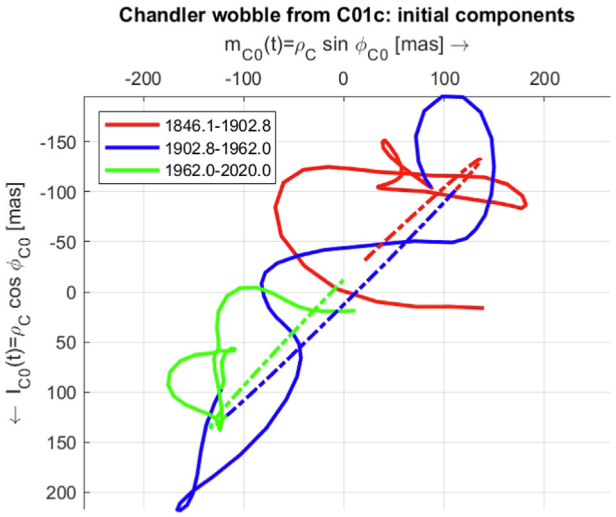

Fig. 18. Initial Chandler components represented as a map. Conventional model with solid lines, alternative model with terms $k = \pm 1$ in Eqs. (17) as dash-dot lines.

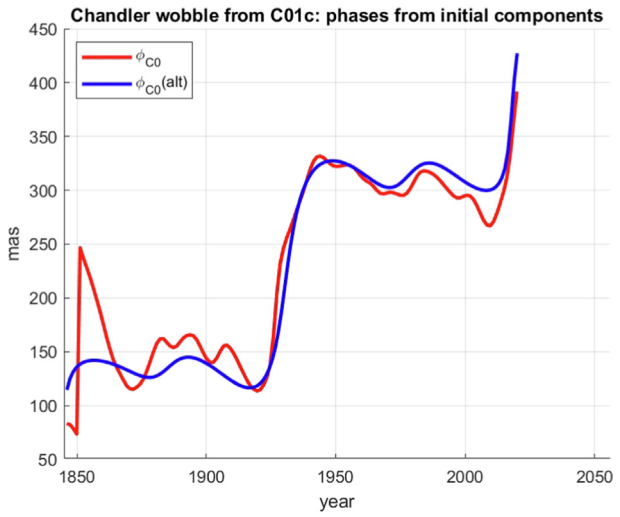

Fig. 19. Phase angles from initial Chandler components. Conventional model with red lines, alternative model with terms $k = \pm 1, \pm 3, \pm 5$ in Eqs. (17) with blue lines. (For interpretation of the references to color in this figure legend, the reader is referred to the web version of this article.)

model (17) as red bars, as a function of their period. The RMS of the fit is provided in the title. For $n = 12$, the value of 41.2 mas is very close to the value achieved with the conventional model (41.4 mas). When only estimating one constant Chandler amplitude ($n = 0$) the RMS of the fit is 112.3 mas, when using the two component model with $k = \pm 1$ it is 64.8 mas, implying that the quality jump from the one- to the two-component Chandler model is substantial. The green "+" symbols mark the $1 - \sigma$-limits of the amplitudes' formal errors. The figure only provides the results for model (17) with $n = 12$. The two dominating amplitudes are those of the original Chandler two-component model. Chandler's amplitudes were quite different, 0".14 for the term with the shorter period, 0".09 for the term with the longer period, whereas our estimates differ by only 15%, with amplitudes of about 85 mas for the term with the shorter period, of about 100 mas for the term with the longer period.

The variation of the initial Chandler components is also provided as a geographical map in Fig. 18, where the conventional model is represented by solid lines, the alternative model by dash-dot lines. Fig. 18 only shows the initial Chandler components according to the alternative model (17) with the two terms $k = -1, k = +1$, because the alternative model with all terms up to $n = 12$ results in a curve which is almost the same as that for the standard model. According to this simple alternative model, the Chandler components move in a highly eccentric ellipse in the retrograde sense around the origin $(l_0, m_0) = (0, 0)$. Note, however, that the sense of rotation is not well determined for highly eccentric ellipses. According to Eqs. (23) the ellipse would even degenerate into a straight line if the amplitudes of the two terms would be the same. Obviously, the sense of rotation would not be defined, in this case. When including more terms in the alternative model, the combined phase motion is prograde, as in the case of the classic model.

It was our approach to analyze the initial components of the Chandler motion. We found the main period as $\tilde{P} \approx 180$ years and consequently the harmonic periods as $\tilde{P}/i, i = 2, 3, \ldots$. We then showed that the long-term periods in the initial Chandler amplitudes are half the periods found for the components. Zotov et al. (2019), in their analysis of the C01 Chandler amplitudes, found two periods of 80 years and 40 years. In view of the difficulties to establish such long periods, our results for the Chandler amplitude variations are undoubtedly consistent with those found by Zotov and Bizouard (2012). We believe, however, that not only the Chandler amplitudes, but also the Chandler initial components should be analyzed to obtain a full description of the Chandler motion.

For the particular choice of the reference epoch the phase angle is $\phi_C \approx -47.4°$ for the two-component Chandler motion.[10] The initial Chandler components therefore move diagonally in Fig. 18, from (bottom, left) to (top, right), and vice versa. The particular value of the phase angle also explains why the maximum value for both initial components is about 140 mas, the minimum value −140 mas, and the corresponding maximum amplitude about 200 mas (Fig. 16 (top)). If the reference epoch would be shifted continuously over one Chandler period, *all* curves in Fig. 18 would continuously rotate by 360°.

Fig. 19 provides the phase angles derived from the initial Chandler components, based on the standard model as solid red line, based on the alternative model with the six components $k = (\pm 1, \pm 3, \pm 5)$ as solid blue lines. Except for the first years the agreement is good. The discrepancy should not be over-interpreted, as the initial components are rather small, in the first years (Fig. 16).

[10] the value emerges from the two-component model (17) with $k = \pm 1$.

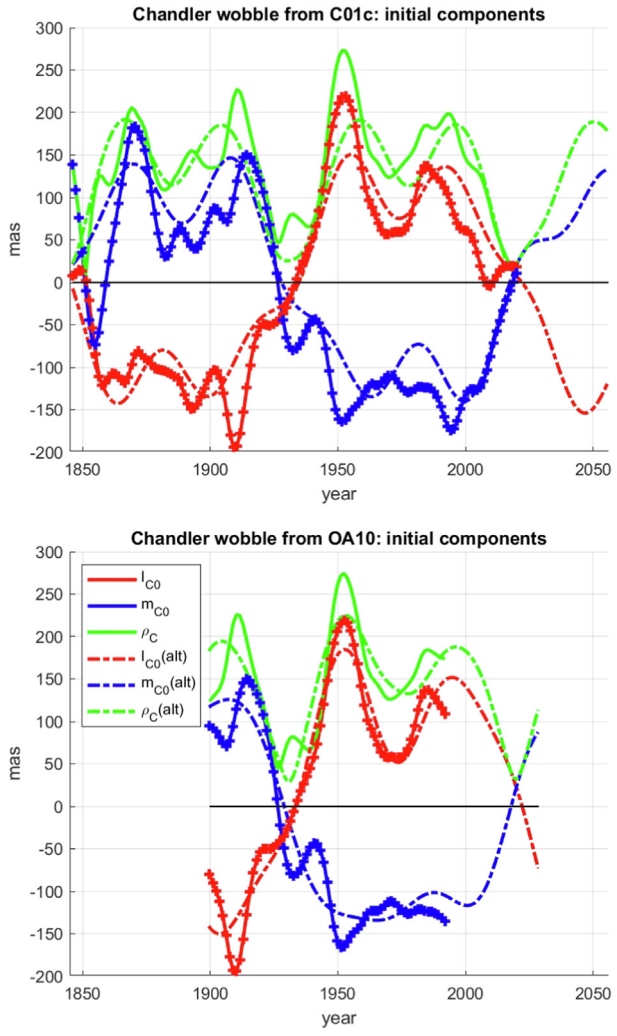

Fig. 20. Prediction of initial Chandler components and amplitudes with alternative model (17) with odd terms $k = \pm1, \pm3, \pm5$. Top: using C01 series, 1846–2019; bottom: using astrometric series OA10, 1900–1992.

Prediction of Chandler motion. The alternative model for the Chandler motion is based on strictly periodic functions, which makes it attractive to extrapolate the Chandler motion beyond the time interval covered by PM observations.

Fig. 20 provides two predictions, one based on the Chandler model derived from the C01 series 1846–2019 (Fig. 20 (top)), one based on the astrometric series OA10 1900–1991 (Fig. 20 (bottom)). "Future" starts in 2020 in the first of the figures, in 1992 in the second. Both figures are based on the alternative model with the six constituents $k = (\pm1, \pm3, \pm5)$ in the alternative model (17). Using the C01 series, the model predicts Chandler amplitudes above 100 mas around 2031 and values of the order of 200 mas around 2045. Is this prediction reliable? Fig. 20 (bottom) may give a clue: the alternative model with the same parametrization predicts the smallest amplitudes around 2020, which is rather close to the period of minimum amplitudes actually observed – not too bad a prediction

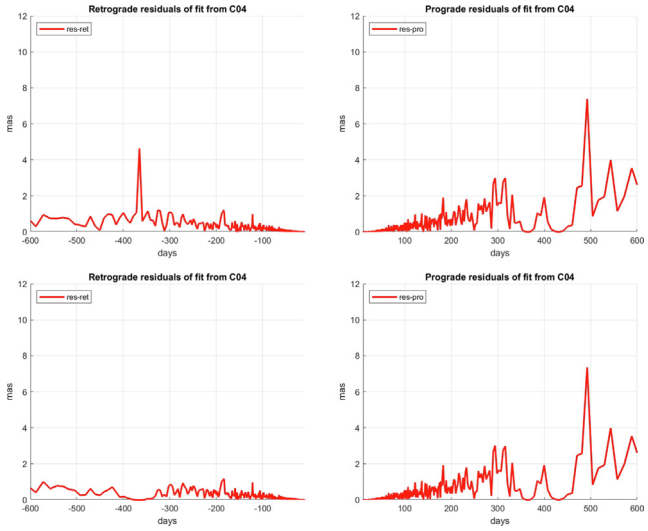

Fig. 21. Residuals of approximating IERS 14 C04 PM in the time interval 1962.0–2020.0 with the standard model. Top: including piecewise linear and continuous mean PM, prograde annual and prograde Chandler initial components as piecewise linear functions of time; bottom: model including in addition retrograde annual PM; left: retrograde part of the spectrum, right: prograde part.

from an astrometry series ending a quarter of a century ago! Amplitudes above 100 mas are predicted for 2027 from optical astrometry, i.e., a few years earlier than the prediction based on space geodesy.

6. Miscellaneous considerations

The three subsections summarize aspects of our article which came up when discussing the first draft of it. Section 6.1 provides additional properties of our standard approximation procedure by discussing the residuals when using exactly the model presented in Section 4 and when generalizing it by solving in addition for retrograde annual motion. Section 6.2 compares our standard method with other empirical procedures used to analyze PM data. Section 6.3 further discusses the splitting of the Chandler frequency and the bifurcation presented in Fig. 15. A simulation study is performed to gain additional insight.

6.1. Residuals of the analysis and extended modeling

When applying the standard model to a particular PM series one obtains not only an approximating function but also the associated residuals. The original data points and the residuals were provided for three PM series in Fig. 2. More insight into the kind of approximation is possible by spectrally analyzing the residuals of the approximation.

Fig. 21 shows the spectra of the residuals when approximating the IERS 14 C04 PM series with the standard model 4, 5, 6, 10 with the settings used in Section 5 for the IERS 14 C04 series. The C04 PM series was selected because it has a length of more than 58 years and because

its accuracy is in essence dominated by the space-geodetic techniques. Figs. 21 (left) show the retrograde part, Figs. 21 (right) the prograde part of the spectra. Figs. 21 (top) use the same model as in Section 5, Figs. 21 (bottom) model in addition the retrograde annual terms. The standard deviation of the fit was the same in both cases (15.1 mas). The only differences in Figs. 21 (top) and 21 (bottom) concern the retrograde annual term at 365.25 days, which were obviously removed in the extended model. As the other model parameters are only marginally affected by this model difference, the decision was made to base the results of the present analysis on circular prograde Chandler motion and to leave the discussion of retrograde PM to future investigations. The figure also indicates, why we modeled the Chandler motion without a retrograde constituent.

Figs. 21 indicate that no serious deficits exist in our model. The standard deviation of the residuals of the C04 PM positions is 15.1 mas for both solutions. The figures also tell that signals in a relatively broad range, 50 mas for the annual prograde and 70 mas for the Chandler motion, were removed around the nominal periods. The retrograde annual period in Fig. 21 (bottom, left) shows a similar behavior as the prograde counterparts. Figs. 21 indicate how the model might be generalized, namely by adding empirical periodic terms in the prograde part around 300 days and 500 days. When doing that the standard deviation of the fit drops below 10 mas.

The voidness of the residual spectra around the annual and Chandler periods tells, that virtually the entire information in these bands has been absorbed by the standard model. This is interesting because the initial components of the Chandler and the annual motions are heavily constrained, i.e., are allowed to vary only slowly.

6.2. Our standard model compared to other smoothing techniques

Why introduce a "new" model to analyze long PM series and why not use more conventional methods like moving averages (boxcar) filters, Gaussian filters, etc.?

Our motivation was to represent PM by a set of well-defined empirical functions characterized by relatively few parameters, which are estimated in one and the same process from the observed PM data. When interested "only" in the long-term development of PM, these estimated parameters sets may be further analyzed instead of the original observations. "Relatively few" means "few compared to the number of original data points". Let us briefly review a few aspects related to the methodology.

It is easily possible to construct time series of parameters of the six PM parameters in Eqs. (3) using a boxcar or moving average filter with a user-defined width. Note that this filtering has to be done simultaneously for all six parameters. Such a procedure with a window width of 8.5 years was used by Vondrák (1999), who modeled the mean PM components within each windows as a linear function of time, the other parameters as constants. He included retrograde annual and retrograde Chandler motion in his model. For the sake of simplicity we stick to Eqs. (3) with their six parameters – thus also modeling mean PM with two mean coordinates within each window. Also, we neglect retrograde annual and Chandler motion.

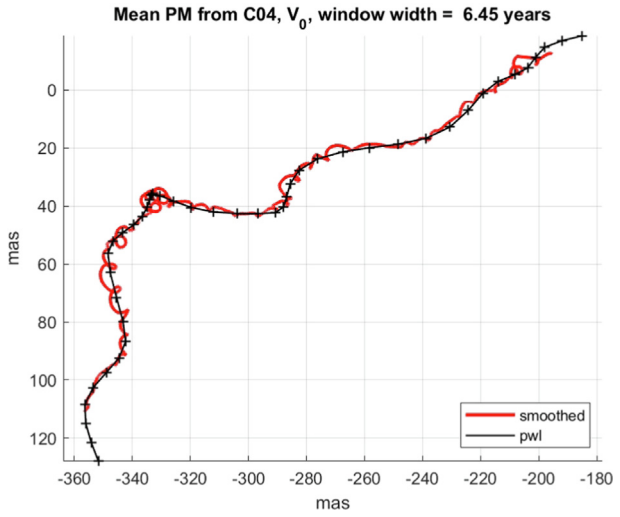

Fig. 22. Mean PM in mas when applying the standard model (black) and the moving average filter with a window width of 6.45 years (red) to the IERS 14 C04 PM series from 1962.0–2020.0. (For interpretation of the references to color in this figure legend, the reader is referred to the web version of this article.)

Let us compare the results achieved with the two methods, i.e., the standard model based on Eqs. (3), (5), (10) the method with the moving average filter with a window width of 6.45 years, when applied to the IERS 14 C04 series (Table 1) from 1962.0 to 2020.0 with a daily spacing of PM values. In the standard method the sub-interval length was set to about 1.3 years and the smoothing factor to $f = 10$.

Fig. 22 overlays the mean PM curves emerging from the standard method (black) and from the moving average filter (red). As the moving average needs about 3.2 years of input data on both sides of the central window epoch, data points for 3.2 years are missing at the beginning and the end of the PM series in the red curve of Fig. 22. When representing the six parameters as linear functions of time and not as constants, the gaps could be filled.

The two types of results agree well in general and in essence result in the same mean PM. Let us point out in particular that the previously discussed sharp bend around 1996.0 is clearly visible in both cases. Note, however, that the moving average in Fig. 22 contains residual effects departing from a really smooth motion due to the strong long-term variations of the Chandler amplitudes. The size of these effects might be substantially reduced by modeling mean PM and the initial components of the Chandler motion as linear functions of time and by enlarging the window width of the filter.

Let us point out that the black curve in Fig. 22 represents an approximating functions with a number n_p of

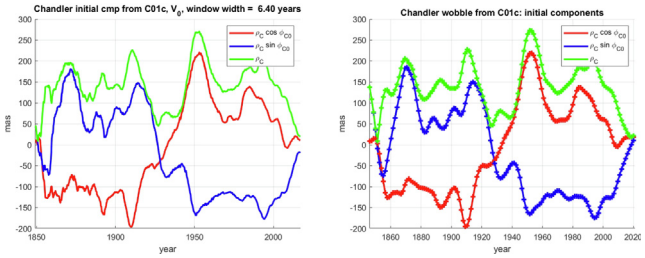

Fig. 23. initial Chandler components resulting from the a moving average with a window width of 6.45 years (left) and from the standard method (right) when applied to the IERS C01 IAU2000 from 1846.0 to 2020.0.

parameters which is much smaller than the number of data points, whereas the red curve is simply a series of averaged data points. Each data point in the original series is used exactly once in the standard model, whereas each original data point is used many times in the moving average.[11] One obtains by design a strictly linear motion between the subinterval boundaries (black crosses) for the black curve, whereas the excursions in the red curve are due to non-modeled effects in the observations. The smoothing of the moving average filter would be perfect, if the motion within each subinterval would be linear in time in each mean PM component. The red curve around the sharp bend in 1995–1996 illustrates the problem of defining meaningful mean PM at that time (see Fig. 6).

Fig. 23 illustrates the application of the two methods to the (corrected) IERS C01 series from 1846.0 to 2020.0. The two methods give highly consistent results. Each data point in Fig. 23 (left) might easily be used to determine the parameters of the alternative model for the Chandler motion (17), whereas we subtracted the estimated mean PM and the annual constituents of PM from the input observations for that purpose when using our standard method. Figs. 23 (left, right) tell that the long-term behavior of the initial Chandler components resulting from the C01 series is *not* a method-specific artifact. Note, however, that the filtered data points in Fig. 23 (left, right) might be used to estimate the parameters of the alternative model.

It is straight forward to replace the boxcar filter used in this section by filters based on different kinds of linear combinations of data points in the moving windows, consult, e.g., Press et al. (1996). Studying the impact of different kinds of windows to PM studies is, however, out of the scope of the present study. Let us mention, however, that the mean pole in (Dick and Thaller, 2016, Fig. 1, Section 3.5.1) was generated by applying a Gaussian filter to the C01 PM series.

As the technique is well established in fundamental astronomy, it is appropriate to mention the Vondrák smoothing, documented in (Vondrák, 1969; Vondrák, 1977), at this point in time. Vondrák smoothing locally[12] represents data points by a polynomial of degree 3. The number of polynomials for the analyzed time series thus in essence equals the number of subintervals between the data points of the analyzed series. Using the Lagrange representation each polynomial is represented by its values at four adjacent data epochs. Smoothing is performed by imposing constraints on the third differences of adjacent smoothed data points, which are the parameters of the process. Vondrák (1969) mentions the two boundary cases of this type of constraining: when the constraints are absent, "0", the filtered data points are identical with the input data points. If the constraints are "∞", the filtered data points represent the best-fitting parabola (polynomial of degree 2) of all data point. As opposed to that, the heavily constrained case is represented by a straight (polynomial of degree 1) in our method. It is another essential difference of the method used here and of the Vondrák smoothing that the number of parameters is much smaller in our case: for a sampling rate of one data point per day and a subinterval length of 1.3 years the number of parameters is about $1.3 \cdot 365 \approx 475$ times smaller in our method. Studying the mutual performance, in terms of results and efficiency, of the two filters is out of the scope of the present study.

6.3. A simulation study

Fig. 24 illustrates a test related to the alternative model (17), where only the terms $k = \pm 1$ were used in the simulation process. Two Chandler-like signals separated by 5.7 days in period, corresponding to a beat period of 180 years, and radii of $\rho_{C\pm1} = 100$ mas were assumed. The phase angles associated with the two constituents were defined in such a way that one of the zero crossings of the initial Chandler components took place in 1924 – the other two therefore occurred near 1834 and 2014. The mean PM components were assumed to move on a straight line, the annual component was assumed to have a constant amplitude of $\rho_a = 100$ mas. Mean PM and the annual initial components had to be estimated, but are not documented here. Daily values of PM between 1830.0 and 2021.0 were simulated.

The simulated PM series was then analyzed with our standard tool using the settings of Section 5.2. Fig. 24 (top, left) contains a 3-dimensional illustration of the simulated data; it roughly resembles the actually monitored PM represented by the C01 series. Fig. 24 (top, right) shows the estimated initial Chandler components when applying our standard method to the simulated PM series. The initial Chandler components estimated with the simulated PM series are similar to the dash-dot lines in Fig. 16 which was generated using real PM data. Figs. 24 (center, left, right) show the amplitude spectra of the simulated

[11] with a window width of 6.45 years and with one data point per day, a particular observation is used in $6.45 \cdot 365.25 \approx 2356$ subsequent filter steps.

[12] within each subinterval defined by two subsequent epochs of the analyzed time series.

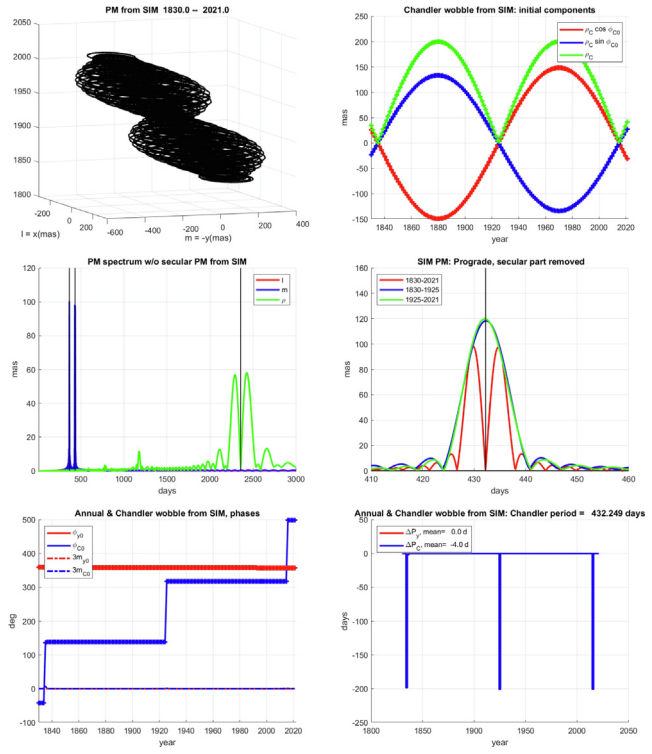

Fig. 24. Analysis of a simulated PM series 1830.0–2021.0 consisting of two sin-waves separated by 5.7 days in period around the nominal Chandler period; top, left: 3-dimensional representation of PM; top, right: estimated initial Chandler components; center, left: spectrum of PM amplitudes; center, right: spectrum of prograde part of PM spectrum using entire time period (red), first half (blue), second half (green); bottom, left: phases from estimated initial Chandler amplitudes; bottom, right: Chandler period changes from phases. (For interpretation of the references to color in this figure legend, the reader is referred to the web version of this article.)

PM series. A comparison with Figs. 15 shows striking similarities. We conclude that Figs. 15 in essence reflect the properties of the alternative model (17) with $k = \pm 1$, which represents Chandler's model (Chandler, 1901). Fig. 24 (bottom, left) shows the phases calculated from the initial Chandler components in Fig. 24 (top, right). The figure shows constant phases except at the epochs when the initial Chandler components are zero: at these epochs the phase "jumps" by 180°. The changes of the Chandler periods calculated from the phase changes are shown in Fig. 24 (bottom, right). The phase jumps obviously correspond to large changes in the Chandler period, as it was also seen in the analysis of real data (Fig. 12). Obviously large changes of the Chandler periods correspond to the zero crossing epochs of the initial Chandler components. Not unexpectedly, the period changes are closer to the zero crossing epochs and they are larger in the simulation than they are in reality.

In summary, Fig. 24 documents that the simple (Chandler, 1901)-model of PM with the appropriate settings has striking similarities with real PM. Together with the argumentation in Section 5.2 we have therefore shown that the alternative model for the Chandler motion, in particular if used to a higher order, is well suited to describe the long-term development of the Chandler motion, including its prediction.

This subsection of course does not prove that the Chandler motion shows "a splitting of the Chandler frequency, as a normal mode frequency". Together with Section 5.2 it shows, however, that real Chandler motion may be rather accurately represented by our alternative model (17). It would be interesting to analyze the PM time series based on solving the Liouville-Euler equations, e.g., those resulting from the analyses (Zotov et al., 2019) or (Ron et al., 2019), with the tools used here.

7. Summary, conclusions, and outlook

The two coordinates of PM are modeled as the superposition of mean PM and the corresponding components of the annual and the Chandler constituents. The Chandler constituent may be modeled in two ways, referred to as the "standard" and the "alternative" analysis, respectively.

The standard analysis. The empirical model to analyze long PM time series was defined in Section 4. Both PM coordinates are defined as the sum of piecewise linear mean PM, or polar wander, and the prograde periodic annual and Chandler motions with nominal periods of 365.25 and 432.25 days, respectively. The amplitudes and phases of the annual and Chandler motions are allowed to vary in time. The actually estimated parameters of PM represent time series, which may be estimated without or with regularization.

The alternative analysis. When inspecting the results of the Chandler motion using the standard model 4, 5, 6, 10 we found convincing arguments that Chandler motion can be represented as a superposition of several constituents, separated in period by few days only. This is why the Chandler motion was also modeled with the alternative model (17), which is, as a matter of fact, a generalization of the model proposed by Chandler (1901).

Both models, labeled as "the standard analysis" and "the alternative analysis" decompose the PM components into a slowly and rapidly time varying part. The model parameters refer to the slowly time-varying part in both cases.

The key results:

- **Mean PM using the CODE series.** The CODE ERP series (Table 1) was analyzed once with the deterministic model without regularization and then with two versions of regularization, using the smoothing factors $f = 5$ and $f = 10$, respectively (Fig. 3). All CODE solutions from 1993.6 onwards follow approximately the mean meridian at 13° West.
- **Mean PM using space-geodetic series after 1995.** Mean PM was estimated from seven PM series (CODE, IERS 14 C04, IVS, ILRS, IDS, USNO, and CSR) with one and the same model. The IDS and the CODE series start

in 1993, the ILRS series in 1998, the IVS series in 1984, the USNO series in 1980, the CSR series in 1976, and the C04 series in 1962. All mean PM series are consistent after about 1995 – there seem to be no technique-specific biases.

- **Mean PM using space-geodetic series after 1976.** All series starting prior to 1990 consistently show a sharp bend in PM around 1995–96 (Fig. 5), whereas the CODE and the DORIS series, starting in 1993, do not show such a bend. It is puzzling that the bend happens roughly at the time when GPS and DORIS emerge as new techniques for PM monitoring, when new versions of the ITRF were generated and when VLBI and SLR networks were augmented by new observing sites in remote parts of the world.
- **The velocities of mean PM**, reconstructed from the mean PM positions at the subinterval boundaries, indicate that a linear model for mean PM is not adequate.
- **Mean PM from historic PM series.** The analysis of pre-space-geodetic data, in particular of the IERS C01 PM series and of two series based on optical astrometry, revealed offsets in mean PM between those parts of the C01 series emerging from different analyses and/or observation techniques. Also, the mean rates of mean PM within the C01 parts differ substantially. When removing the offset of the 1900.0–1962.0 part from the currently used C01 version and when taking over the rates from 1900.0–1962.0 to the interval 1846.0–1900.0, a smooth mean PM series from 1846 to 2019 is obtained (Fig. 9).
- **Chandler PM motion.** The two initial Chandler components, estimated from the C01 series, show an eye-catching variation in time with a period of about 180 years. The period of the corresponding amplitudes is half this value, i.e., about 90 years.
- **Chandler PM motion viewed by the alternative model.** Fig. 16 shows the variations of the initial Chandler components, emerging from model (4), (5) as solid lines, and emerging from the alternative model (17) as dash-dot lines. The alternative model in Fig. 16 (top) represents the two-component model as originally proposed by Chandler (1901) – with different periods and amplitudes. The Chandler model of 1901 actually captures the two dominating terms of long-period polar motion. In a slight modification of Chandler's statement in 1901 we believe "to have given overwhelming evidence for the fine structure of the Chandler motion represented by Eqs. (17)".
- **Prediction of Chandler motion.** The alternative model for Chandler motion is well suited to predict the initial coordinates and amplitudes of the Chandler part of PM over a few decades (Fig. 20).

Outlook and conclusions. The sharp bend of mean PM around 1995–96 should be further analyzed. The VLBI and SLR solutions and the underlying assumptions concerning the terrestrial reference frame(s) should be studied in detail. We have put a rather reliable time-tag (1995/96) on this bend. A review of the SLR and VLBI solutions might reveal whether the bend in mean PM around 1995–96 is real or caused by substantial changes in the observation methods and analysis strategies used.

The experiments performed indicate that the Chandler motion can be modeled as a superposition of several constituents, separated in period by few days. The main period seen in the components of Chandler motion referring to a particular epoch lies between 170 and 190 years, the main period in the amplitude is half this value, about 85–95 years. The latter value corresponds to the beat period of the two dominating Chandler terms.

Declaration of Competing Interest

The authors declare that they have no known competing financial interests or personal relationships that could have appeared to influence the work reported in this paper.

Acknowledgements

We cordially thank Heinz Spahni for the thorough review of all manuscript versions and for his most valuable contributions to the development of what was called here "the alternative model" for describing the Chandler motion.

The first also author wishes to thank Reiner Rummel for carefully reading the manuscript and for many inspiring discussions.

The "recent" technique-specific PM series analyzed here originate directly or indirectly from the scientific IAG Services IDS, ILRS, IGS, and IVS, documented in (Willis et al., 2016; Pearlman et al., 2002; Johnston et al., 2017; Nothnagel et al., 2017). The combined C04- and C01-series were compiled by the IERS.

The astrometric series OA00 and OA10 were received directly from Jan Vondrák, Prague. Cordial thanks go to him and to all colleagues supporting our effort knowingly or unknowingly. Without the competence and the dedication of the organizations and the individuals collaborating in the scientific IAG services, and their predecessor organizations, like BIPM and ILS, Polar Motion monitoring would not exist.

We thank Christian Bizouard and two anonymous reviewers of this manuscript. Their constructive remarks greatly helped to improve the paper.

Last but not least we would like thank the ASR Editor in Chief Pascal Willis, who not only helped to cure formal inconsistencies, but also initiated the correct interpretation of the DORIS-derived mean PM illustrated by Fig. 6.

References

Altamimi, Z., Rebischung, P., Métivier, L., Collilieux, X., 2016. ITRF2014: a new release of the International Terrestrial Reference Frame modeling nonlinear station motions. JGR Solid Earth 121, Issue 8.

Barnes, R.T.H., Hide, R., White, A.A., Wilson, C.A., 1983. Atmospheric angular momentum fluctuations, length-of-day changes and polar motion. Proc. R. Soc. Lond., A 387, 31–73.
Beutler, G., 2005. Methods of Celestial Mechanics. Springer-Verlag, Berlin, Heidelberg, New York.
Bizouard, Ch., Remus, F., Lambert, S.B., Seoane, L., Gambis, D., 2011. The Earth's variable Chandler wobble. Astron. Astrophys. 526, A106. https://doi.org/10.1051/0004-6361/201015894.
Bizouard, Ch., Remus, F., Lambert, S.B., Gattano, C., Becker, O., Richard, J.-Y., 2018. The IERS EOP 14C04 solution for Earth orientation parameters consistent with ITRF 2014. JoG. https://doi.org/10.1007/s00190-018-1186-3, on line.
Bizouard, Ch., 2018. Private communication.
Bizouard, Ch., 2020. Geophysical Modelling of the Polar Motion. De Gruiter Studies in Mathematical Physics, 31, in print. publication planned Oct. 2020.
Brzezinski, A., 1994. Polar motion excitation by variations of the effective angular momentum function: II. Extended Model. Manuscripta Geodaetica 19, 157–171.
Carter, M.S., Carter, W.E., 2000. Seth Carlo Chandler Jr.: The Discovery of Variation of Latitude. In: Dick, S., McCarthy, D., Luzum, B. (Eds.), Polar Motion: Historical and Scientific Problems, Astronomical Society of the Pacific (ASP) Conference Series, vol. 208.
Chandler, S.C., 1901. On a new component of the polar motion. Astron. J. 490, 79–80.
Chandler, S.C., 1891a. On the Variation of Latitude, I 248, 59–61.
Chandler, S.C., 1891b. On the Variation of Latitude, II 249, 65–70.
Chandler, S.C., 1892a. On the supposed variation of latitude 255, 113–116.
Chandler, S.C., 1892b. On the Variation of Latitude, VII 277, 97–101.
Chen, J.L., Wilson, C.R., Ries, J.C., Tapley, B.D., 2013. Rapid ice melting drives the Earth's pole to the east. Geophys. Res. Lett. 40, 2625–2630. https://doi.org/10.1002/grl.50552.
Dach, R., Brockmann, E., Schaer, S., Beutler, G., Meindl, M., Prange, L., Bock, H., Jäggi, A., Ostini, L., 2009. GNSS processing at CODE: status report. J. Geod. 83 (3–4), 353–366. https://doi.org/10.1007/s00190-008-0281-2.
Dach, R., Lutz, S., Walser, P., Fridez, P., (Eds.), 2015. The Bernese GPS software version 5.2. Astronomical Institute, University of Bern, doi: 10.7892/boris.72297.
Dick, R., Thaller, D. (Eds.), 2016 IERS Annual Report 2015. International Earth Rotation and Reference Systems Service, Central Bureau, Bundesamt für Kartographie und Geodäsie, Richard-Strauss-Allee 11, 60598 Frankfurt am Main, ISBN: 978-3-86482-087-8.
Euler, L., 1766: Recherches sur le mouvement de rotation des corps célestes. HARSB, 15(1759), 265–309; LEOO, II, 29:220–256. HARSB = Histoire de l'Académie Royale des Sciences et Belles-Lettres (Berlin), LEOO = Leonhardi Euleri Opera Omnia.
Fedorov, E.P., Yatskiv, Ya S., 1965. The cause of the apparent "bifurcation" of the free nutation period. Soviet Astron. AJ 8 (4), 608–611.
Fedorov, E.P., Korsun, A.A., Major, S.P., Panchenko, N.T., Tarady, V. K., Ya, A., Yatskiv, 1972. New determination of the polar motion from 1890 to 1969. In: Melchior, P., Yumi, S. (Eds.), IAU Symposium No. 48 Rotation of the Earth, pp. 12–13.
Gross, R.S., Vondrák, J., 1999. Astrometric and space-geodetic observations of polar wander. GRL 26 (14), 2085–2099.
Gross, R.S., 2007. Earth Rotation Variations – Long Period. Physical Geodesy, Ed. TA Herring, Treatise on Geophysics, vol. 3. Elsevier. ISBN: 0444534601 (Chapter 11).
Guinot, B., 1972. The Chandlerian wobble from 1900–1970. Astron. Astrophys. 19, 207–214.
Höpfner, J., 2004. Low-frequency variations, Chandler and Annual wobbles of polar motion as observed over one century. Surv. Geophys. 25, 1–54.
Jeffreys, H., 1940. The variation of latitude. Mon. Not. R Astron. Soc. 100, 139–155.
Johnston, G., Riddell, A., Hausler, G., 2017. The International GNSS Service. In: Teunissen, P.J., Montenbruck, O. (Eds.), Springer Handbook of Global Navigation Satellite Systems. Springer, International Publishing, Cham, Switzerland, pp 967–982.
Küstner, F., 1888. Neue Methode zur Bestimmung der Aberrations-Constante nebst Untersuchungen über die Veränderlichkeit der Polhöhe. Beobachtungs-Ergebnisse der Königlichen Sternwarte zu Berlin 3, 1–59 (in German).
Lambeck, K., 1980. The Earth's variable rotation: Geophysical causes and consequences. Cambridge University Press.
Malkin, Z., Miller, N., 2011. Chandler wobble: two more large phase jumps revealed. Earth Planets Space 62, 943–947. https://doi.org/10.5047/eps.2010.11.002.
McCarthy, D.D., Petit, G., 2003. IERS Conventions (2003). IERS Technical Note 32, Verlag des Bundesamts für Kartographie und Geodäsie, Frankfurt am Main, Germany. ISBN: 3-89888-884-3
McCarthy, D.D., Seidelmann, K.P., 2009. Time from EarthRotation to Atomic Physics. Wiley-VCH Verlag, Weinheim, Germany, ISBN: 978-3-527-40780-4.
Moreaux, G., Lemoine, F.G., Capdeville, H., Kuzin, S., Otten, M., Štěpánek, P., Willis, P., Pascale Ferrage, P., 2016. The International DORIS Service contribution to the 2014 realization of the International Terrestrial Reference Frame. ASR 58, 2479–2504.
Munk, W.H., McDonald, G.J.W., 1960. The Rotation of the Earth. A Geophysical Discussion. University Press, New York.
Nothnagel, A., Artz, T., Behrend, D., Malkin, Z., 2017. International VLBI Service for geodesy and astrometry: delivering high-quality products and embarking on observations of the next generation. JoG 91 (7), 711–721.
Pearlman, M., Degnan, J., Bosworth, J., 2002. The international laser ranging service. ASR 30 (2), 135–143.
Petit, G., Luzum, B., 2010. IERS Conventions (2010). Verlag des Bundesamtes für Kartographie und Geodäsie, Frankfurt, Germany, IERS Conventions Centre.
Plag, H.-P., Chao, B., Gross, R., Van Dam, T. (Eds.), 2005. Forcing of polar motion in the Chandler frequency band: A contribution to understanding interannual climate variations, Cahiers du Centre Européen de Géodynamique et de Séismologie 24.
Press, H.W., Teukolsky, S.A., Vetterling, W.T., Flannery, B.P., 1996. Numerical Recipes in Fortran 77 – The Art of Scientific Computing, second ed. Cambridge University Press, Cambridge.
Ron, C., Vondràk, J., Dill, R., Chapanov, Ya, 2019. Combination of geomagnetic jerks with updated ESMGFZ effective angular momentum functions for the modelling of polar motion excitation. Acta Geodyn. Geomater. 16(4)(196), 359–363, 2019, doi: 10.13168.
Roy, K., Pelletier, W.R., 2011. GRACE era secular trends in Earth rotation parameters: A global scale impact of the global warming process? Geophys. Res. Lett. 38, L10306. https://doi.org/10.1029/2011GL047282.
Rykhlova, L.V., 1969. Motion of the Earth's pole 1846–1991.5, from observations at Pulkovo. Soviet Astronomy – AJ, vol. 12, no. 5, March-April 1969.
Schuh, H., Nagel, S., Seitz, T., 2001. Linear drift and periodic variations observed in long time series of polar motion. J. Geodesy 74, 701–710.
Seitz, F., Schmidt, M., 2005. Atmospheric and oceanic contributions to Chandler wobble excitation determined by wavelet filtering. JGR 110, B11406.
Seitz, F., Müller, J., 2016. Erdrotation. In: Erdmessung und Satellitengeodäsie, Herausgeber Reiner Rummel, Springer Reference Naturwissenschaften. Springer Spektrum, ISBN, ISBN 978-3-662-47100-5.
Vicente, R.O., Wilson, C.R., 2005. The need for a new definition of a conventional international origin. J. Geod. 79, 269–279. https://doi.org/10.1007/s00190-005-0469-7.
Verdun, A., Beutler, G., 2000. Early Observational Evidence of Polar Motion. Astronomical Society of the Pacific (ASP) Conference Series, Vol 208, 67–81, Eds. Dick S, McCarthy D, Luzum B.
Vondrák, J., 1969. A contribution to the problem of smoothing observational data. Bull. Astron. Inst. Czechosl. 20, 349–355.

Vondrák, J., 1977. Problem of smoothing observational data II. Bull. Astron. Inst. Czechosl. 28, 84–89.
Vondrák, J., Ron, C., Pešek, I., Čepek, A., 1995. New global solution of Earth orientation parameters from optical astrometry in 1900–1990. Astron. Astrophys. 297, 899–906.
Vondrák, J., 1999. Earth rotation parameters 1899.7–1992.0 after reanalysis within the Hipparchos frame. Surv. Geophys. 20, 169–195 (Kluwer Academic Publishers).
Vondrák, J., Ron, C., Pešek, I., 2000. Survey of observational techniques and HIPPARCOS reanalysis. Int. Astron. Union Colloquium 208. https://doi.org/10.1017/S0252921100061376.
Vondrák, J., Ron, C., 2005. The great Chandler wobble change in 1923–1940 re-visited. Cahiers du Centre Européen de Géodynamique et de Séismologie 24, 39–47.
Vondrák, J., Ron, C., Štefka, V., 2010. Earth Orientation Parameters based on EOC-4 Astrometric Catalogue. Acta Geodyn. Geomater. 7 (1 (157)), 245–251.
Wahr, J., Nerem, R.S., Bettadpur, S.V., 2015. The pole tide and its effect on GRACE time-variable gravity measurements: Implications for estimates of surface mass variations. J. Geophys. Res. Solid Earth 120, 4597–4615. https://doi.org/10.1002/2015JB011986.
Willis, P., Lemoine, F.G., Moreaux, G., Soudarin, L., Ferrage, P., Ries, J., Otten, M., Saunier, J., Noll, C., Biancale, R., Luzum, B., 2016. The International Doris Service (IDS): Recent developments in preparation for ITRF2013. In: Rizos, C., Willis, P. (Eds.), IAG 150 Years. Springer International Publishing, pp 631–640.
Zotov, L., Bizouard, D., 2012. On modulations of the Chandler wobble excitation. J. Geodyn. 62, 30–34.
Zotov, L., Bizouard, D., Sidorenkov, N., 2019. Chandler wobble variability. Journees-2019, Paris. https://syrte.obspm.fr/astro/journees2019/journees_pdf/SessionIV_2/ZotovJournees19.pdf.
Zotov, L., 2019. Study of the Links Between the Earth Rotation and Geophysical Processes Doctoral thesis. Lomonosov Moscow State University (in Russian).